and increased upon fasting in the mutant liver. These results suggest that GATE-16 may be constitutively degraded even at fed condition in heterozygous mice and up-regulated in response to fasting under defective *Atg7*. The levels of all LC3 homologues were elevated even at fed condition in the mutant liver, suggesting their marked stabilization in autophagy-deficient condition. However, the possibility that their transcriptions are up-regulated at basal level due to *Atg7* deficiency cannot be excluded. We sought to determine their localizations in the cells. However, our antibodies for these molecules were not applicable for immunofluorescent analyses, and those localizations remain to be clarified. In conclusion, all Atg8 homologues respond to fasting, although in a different manner, and their levels are affected by the absence of Atg7.

Atg7 is indispensable for fasting-induced degradation of cytosolic proteins and organelles in the mouse liver

Given that autophagosome formation was impaired in *Atg7*-deficient liver, we next examined its effects on the bulk degradation of proteins and organelles under fasting condition. After 1-d fasting in control $Atg7^{F/+}$:Mx1 and mutant $Atg7^{F/F}$:Mx1 mice, the liver was dissected and the amount of total protein per whole liver was measured. The amount of total liver proteins decreased to ~66% by 1-d fasting in the control liver (Fig. 4 A). In contrast, fasting did not significantly decrease the amount of total liver proteins in the mutant liver. Moreover, the amount of total proteins in the mutant liver was 1.5-fold that of control. These results indicate that the decrease of total proteins is dependent on Atg7 and autophagosome formation.

We also examined whether or not fasting causes the degradation of cellular organelles such as mitochondria in the livers of mice. To quantify the amount of the mitochondria, we first measured the activity of mitochondrial enzyme succinate dehydrogenase (SDH) in total liver extracts. In the control livers, fasting was associated with a significant decrease of SDH activity, and the reduction was proportional with the decrease in the amount of total protein (Fig. 4 B). In contrast, fasting was not associated with any change in SDH activity in the mutant livers. Similar to total protein, the basal SDH activity in mutant liver was significantly higher than in control. The effect of fasting on the amount of the mitochondria was also assessed by immunoblot analysis of mitochondrial protein cytochrome *c* (Fig. 4 C). When equal amounts of proteins were loaded, the level of cytochrome *c* was equivalent in the two genotypes at either fed or fasting conditions, suggesting that the ratio of mitochondria versus total protein is not altered by fasting in both genotypes. Considering that the total protein amounts decreased by fasting in the control liver (Fig. 4 A), these results suggest that the mitochondria and cytoplasmic proteins are proportionally degraded upon fasting in heterozygous mice. However, such degradation is impaired in *Atg7*-deficient liver because the levels of both proteins and mitochondria are unchanged and kept at a higher level.

Next, we investigated the effect of autophagy deficiency on protein turnover. To quantify the turnover of long-lived protein, after each control and mutant hepatocytes had been labeled with [^{14}C]leucine for 24 h and chased for 2 h, the release of TCA-soluble [^{14}C]leucine was measured for 4 h. In control hepatocytes, nutrient deprivation significantly induced protein degradation, and such degradation was suppressed by the addition of lysosomal inhibitors such as monomethylamine and E64d and pepstatin (Fig. 4 D). The induced degradation was still observed in the presence of proteasome inhibitor epoxomicin, suggesting that such protein degradation is mediated in the lysosomal pathway rather than the proteasome (Fig. 4 D). In the mutant hepatocytes, degradation of long-lived protein was not induced by nutrient deprivation (Fig. 4 D), indicating that autophagy is the main route for lysosomal degradation under starvation condition. Consistent with these results, amino acid concentrations in starved mutant hepatocytes were lower than in control hepatocytes (unpublished data). Intriguingly, although lysosomal inhibitors inhibited protein degradation even

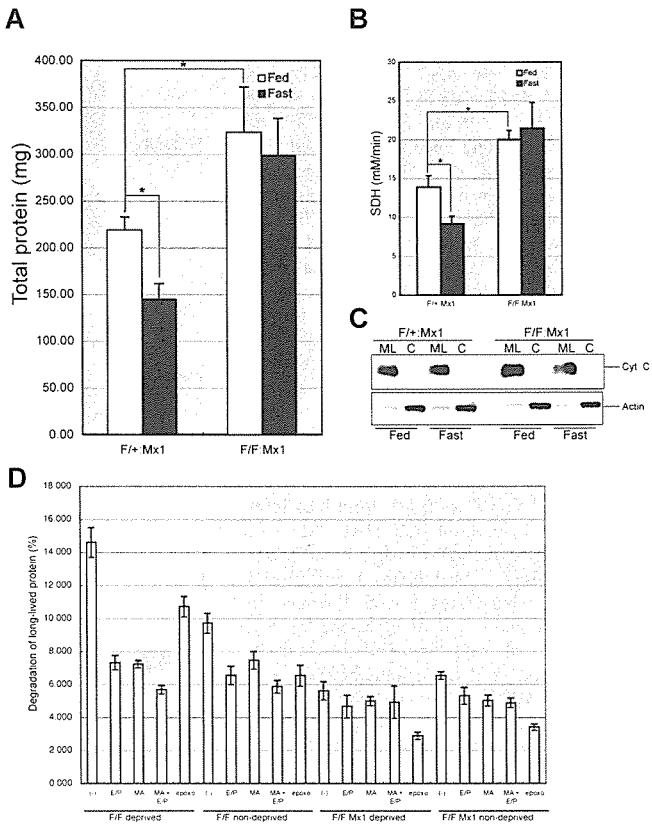

Figure 4. **Fasting response of *Atg7*-deficient liver.** (A and B) Livers from $Atg7^{F/+}$:Mx1 and $Atg7^{F/F}$:Mx1 mice fed ad libitum (Fed) or fasted for 1 d (Fast) at 20 d after pIpC injection were dissected, and the amount of total protein (A) and SDH activity (B) per liver were measured. Data are mean ± SD values of five mice in each group; *, $P < 0.01$. (C) Cytochrome *c* levels in the cytosolic and mitochondria/lysosomal fractions of the liver at 20 d after injection. Equal amount of PNS fractions were centrifuged at 8,000 *g* for 10 min and the pellets were used as the mitochondrial/lysosomal fraction (ML). The supernatants were further centrifuged at 100,000 *g* for 1 h and the supernatant was used as the cytosolic fraction (C). Actin was blotted as control. Data shown are representative of two separate experiments. (D) Turnover of long-lived protein. Hepatocytes from $Atg7^{F/+}$:Mx1 and $Atg7^{F/F}$:Mx1 mice were isolated and labeled with [^{14}C]leucine for 24 h, and degradation of long-lived protein in deprived or nondeprived condition was measured. Monomethylamine (MA) and/or E64d and pepstatin (E/P) or epoxomicin (epoxo) was added as indicated. Data are the mean ± SD of triplicate experiments.

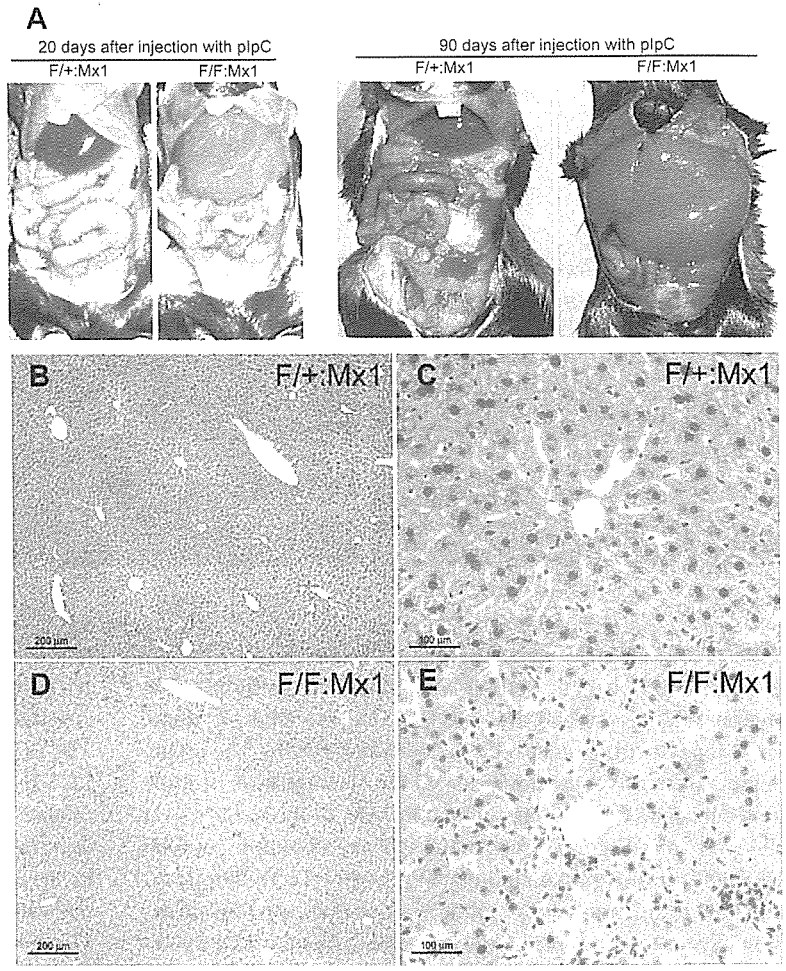

Figure 5. ***Atg7* deficiency in the liver causes hepatomegaly and hepatic cell swelling.** (A) The gross anatomical views of representative mice at the indicated day after pIpC injection. (B–E) Histology of representative livers with *Atg7* deficiency. Hematoxylin and eosin staining of $Atg7^{F/+}$:Mx1 (B and C) and $Atg7^{F/F}$:Mx1 (D and E) liver at 90 d after pIpC injection.

at nondeprived condition in the control hepatocytes, such inhibition was not significant in the mutant hepatocytes (Fig. 4 D), indicating that significant amounts of proteins are constitutively degraded in the lysosome via autophagic pathway. Together, these results suggest that autophagy plays a significant role in turnover of long-lived protein.

Loss of *Atg7* in the liver leads to hepatomegaly and accumulation of abnormal organelles in hepatic cells

We further chased the phenotypes of the mutant mice for up to 90 d after pIpC injection. Gross anatomy revealed severe enlargement of the liver, filling up most of the abdominal cavity (Fig. 5 A). Other major organs were normal histologically (Fig. S3, available at http://www.jcb.org/cgi/content/full/jcb.200412022/DC1). The mean liver weights of control and mutant mice at 90 d after pIpC injection were 1.39 ± 0.24 and 6.10 ± 2.06 g, respectively (n = 5 each). Histological analysis revealed disorganized hepatic lobules and cell swelling in the mutant liver (Fig. 5, D and E). No hepatocellular proliferation or regeneration was detected (unpublished data). Vacuolated hepatic cells were occasionally observed and those were associated with hepatic cell death, which is consistent with the leakage of alkaline phosphatase, aspartate aminotransferase, and alanine aminotransferase in the mutant mice sera (Fig. S4, available at http://www.jcb.org/cgi/content/full/jcb.200412022/DC1).

Although most hepatocytes were still alive in the mutant liver, ultrastructural analysis revealed the appearance of aberrant concentric membranous structures (Fig. 6, A and B), which were also observed as early as 20 d after pIpC-injected liver (not depicted). These structures surrounded various cytoplasmic constituents such as mitochondria, lipid droplets, and vesicular structures (Fig. 6 A). Their membranous elements were continuous with the rough ER (Fig. 6 B, arrowheads), and the corresponding structures were positive for calreticulin, an ER protein marker (not depicted), indicating that these structures originated from the rough ER. Accumulation of peroxisomes (Fig. 6 C) and deformed mitochondria (Fig. 6, C and D) was also observed in the mutant liver. These results suggest the important role of autophagy in turnover of organelles, and its defect results in accumulation of abnormal organelles.

Formation of ubiquitin-positive inclusions in *Atg7*-deficient hepatocytes

Autophagy has been implicated in not only organelle turnover but also in elimination of protein aggregates (Kopito, 2000). Protein aggregates are often ubiquitinated. In the next step, we immunostained the liver with an ubiquitin antibody to examine the presence of such aggregates. Several ubiquitin-positive par-

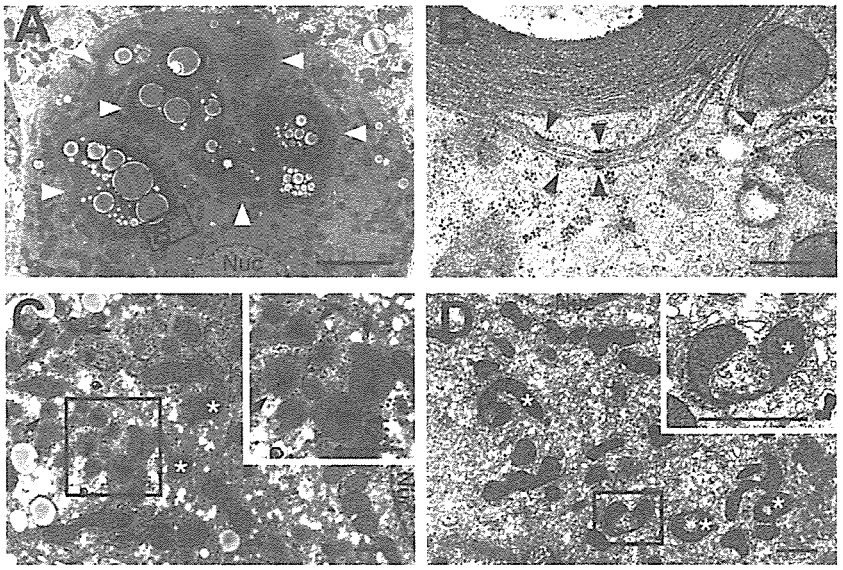

Figure 6. **Electron micrographs of hepatic cells with *Atg7* deficiency.** (A and B) Note the presence of concentric membranous structures in the mutant cells (arrowheads). Higher magnification view (B) shows the membranous elements are continuous with the rough ER (arrowheads). (C and D) The mutant cells contained a high number of peroxisomes (arrows) and deformed mitochondria (asterisks). Insets show higher magnification views. Nuc, nucleus. Bars: (A) 5 μm; (B) 0.5 μm; (C and D) 1 μm.

ticles of various sizes were detected in the $Atg7^{F/F}$:Mx1 but not in $Atg7^{F/+}$:Mx1 hepatic cells at both 10 and 90 d after pIpC injection (Fig. 7, A and B; and Fig. S5, available at http://www.jcb.org/cgi/content/full/jcb.200412022/DC1). The immunoblots of the liver lysates revealed the accumulation of high-molecular mass polyubiquitinated proteins in the mutant liver (Fig. 7 G and Fig. S5), suggesting that the ubiquitin particles are aggregates of polyubiquitinated proteins. To further determine the localization of ubiquitin-positive dots, analysis of immunoelectron micrographs was performed. Numerous particles of colloidal gold, indicative of ubiquitin, were detected on lipid dropletlike structures, membranous structures, and amorphous substances in the cytoplasm (Fig. 7, C–F). Such signals were not observed in the wild-type liver (unpublished data).

The accumulation of ubiquitin-positive inclusions in the cytoplasm prompted us to examine the effect of autophagy deficiency on proteasome function. Immunoblots of proteasome subunits (p112/Rpn2, Mss1/Rpt1, and α5) showed that their relative amounts were not affected in the mutant liver (Fig. 7 G). Furthermore, the activities of the proteasome, measured by Suc-LLVY-MCA as substrate, were also comparable between wild-type and mutant livers (unpublished data). These results indicate the accumulation of ubiquitin-positive aggregates in autophagy-deficient hepatocytes despite the apparently normal proteasome function.

Discussion

Autophagy is a bulk protein degradation pathway, which is conserved in eukaryotes, essential for the survival of unicellular organisms under nutrient-poor condition and for cellular remodeling of multicellular organisms (Mizushima et al., 2002; Levine and Klionsky, 2004). In the present study, we generated conditional knockout mice of *Atg7* gene, which is an essential gene for autophagy in budding yeast, and analyzed its roles in mice.

In mammals, *Atg7* was indeed essential for ATG12 conjugation, LC3 modification systems, and autophagosome formation (Fig. 2, Fig. 3, and Fig. S2). Immunofluorescent analyses revealed that LC3-positive dots appeared but did not form cup-shaped and ringlike structures in $Atg7^{F/F}$:Mx1 livers (Fig. 3). The LC3-I form is usually present at the S100 fraction and the LC3-II form at the P100 fraction (Kabeya et al., 2000). In the mutant liver, LC3-I was present in both S100 and P100 fractions (unpublished data), suggesting that the LC3-positive dots in the mutant hepatocytes are indeed the LC3-I form. These results suggest that LC3 may be recruited to the dot structures independent of the modification (Fig. 3). In mammals, LC3 has at least two homologues, GABARAP and GATE-16, which share common biochemical characteristics (Tanida et al., 2001) and localize to autophagosome in response to fasting (Kabeya et al., 2004). Indeed, the modification and levels of these molecules under fasting condition were affected in the mutant liver (Fig. 3 N). However, these LC3 homologues have been identified in a different biological pathway and may have diverse functions (Ohsumi, 2001). Thus, how their functions and localizations are affected in *Atg7*-deficient cells remains to be clarified.

Although $Atg7^{-/-}$ mice were born at Mendelian ratio, and the major organs were almost normal histologically (Fig. S1), they had reduced body weight and died within 1 d after birth. $Atg7^{-/-}$ mice had lower amino acid level and died earlier compared with wild type under nonsuckling condition after caesarean delivery (Fig. 2 G), suggesting that *Atg7* is important for survival during the early neonatal starvation period, similar to recently reported $Atg5^{-/-}$ mice phenotypes (Kuma et al., 2004). However, because suckling $Atg7^{-/-}$ mice also died within 1 d after birth (unpublished data), the cause of death may not be only due to low level of amino acids. The reason for the reduced body size is also unclear and may be related to placental function or due to inefficient reutilization of nutrients during embryogenesis. It is of note that a lower level of autophagy occurs during embryogenesis (Mizushima et al., 2004) even when nutrients are supplied from the placenta. Furthermore, *Atg7* null mice possess several ubiquitin-positive inclusions in some

organs at the time of birth (unpublished data). This phenotype might be related to the earlier death of mutant. Further analysis of $Atg7^{-/-}$ mice is required to unravel the roles of autophagy, and such analysis is currently under way by breeding the $Atg7^{F/F}$ mice with several Cre-transgenic mice.

Starvation-induced autophagosomes appeared to sequester the cytoplasm randomly (Fig. 3). Consistent with this notion, the amount of mitochondria decreased in proportion with reduction in the amount of total protein (Fig. 4, A–C). These results suggest that mitochondria are degraded nonselectively under fasting condition. In *Atg7*-deficient liver, no autophagosome formation was noted and the degradation of proteins and organelles under fasting condition was largely impaired. These results suggest that the rapid reduction of proteins and organelles upon fasting is dependent on *Atg7* and autophagosome formation.

Although autophagy can be induced by starvation, this pathway may take place even at feeding condition at basal level. This constitutive pathway may be important for turnover of organelles and cytoplasmic proteins. Indeed, the degradation of long-lived protein was inhibited in mutant hepatocytes irrespective of nutrient deprivation (Fig. 4 D), and multiple abnormalities of organelles (e.g., the presence of concentric membranous structure and accumulation of deformed mitochondria) were observed in *Atg7*-deficient hepatocytes (Fig. 6). Unexpectedly, the morphologically abnormal mitochondria appear to retain their function, as judged by the normal membrane potentials and the absence of cytochrome *c* leakage in the cytosol (unpublished data). In contrast to starvation-induced autophagy, whether or not constitutive autophagy eliminates abnormal and excess organelles in a degree of selectivity remains to be clarified.

Beclin 1, a human homologue of *ATG6/VPS30* essential for autophagy in yeast, was recently identified as a tumor suppressor gene, and autophagy has been implicated in the regulation of cellular proliferation (Liang et al., 1999). Indeed, heterozygous disruption of mouse *Beclin 1* led to enhanced tumorigenesis (Qu et al., 2003; Yue et al., 2003). *Atg7* deficiency led to hepatomegaly (Fig. 5 A), suggesting that cell proliferation or malignant transformation might be induced in the *Atg7*-deficient cells. However, neither tumorigenesis nor enhanced cell proliferation was detected as tested by BrdU incorporation at 90 d after pIpC injection in the mutant liver compared with control mice (unpublished data). The hepatomegaly observed in the mutant mice was likely due to increased cellular volume rather than cell number, which is also supported by the swollen appearance of hepatocytes (Fig. 5, D and E).

In *Atg7*-deficient liver, we detected numerous ubiquitin-positive particles indicative of protein aggregates (Fig. 7 and Fig. S5). It has been reported that proteasome inhibition leads to aggregate formation. Conversely, the formation of protein aggregates inhibits the proteasome (Bence et al., 2001), resulting in a malignant cycle of aggregate formation and proteasome inhibition. In the mutant liver, failure of the proteasome was postulated; however, no impairment of proteasome function, in terms of its expression or peptidase activities, was noted (Fig. 7 G and not depicted). Our results suggest that the ubiquitinated proteins eventually aggregate even in the presence of functional proteasomes. Considering that such ubiquitinated aggregates must be difficult to unfold, and proteasomes need to unfold their substrate before degradation (Baumeister et al., 1998), it is likely that elimination of ubiquitin-positive aggregates in the cells is largely dependent on the autophagic process. Protein ubiquitination may also occur after protein aggregation. In either case, we propose the possibility that protein ubiquitination may serve as a signal to the autophagic process in addition to the proteasomes pathway. In this context, it is worth noting that sperm mitochondria are known to be ubiquitinated before degradation during fertilization (Sutovsky et al., 1999). It is now well established that ubiquitin regulates not only proteasomal degradation, but also lysosomal degradation. Thus, it is conceivable that ubiquitin could also regulate the autophagic pathway.

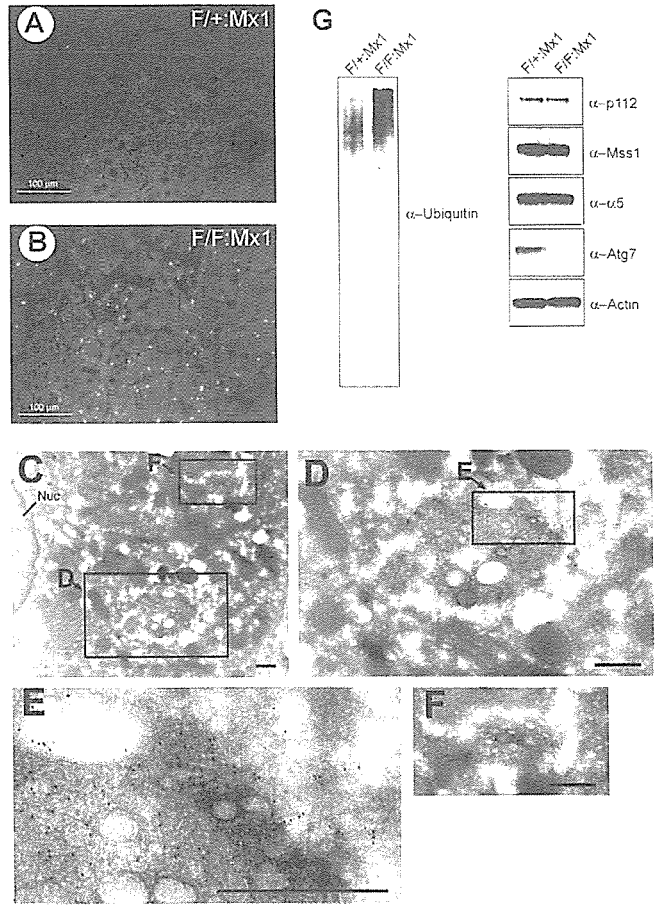

Figure 7. **Accumulation of ubiquitin-positive aggregates in *Atg7*-deficient liver.** (A and B) Immunofluorescent detection of ubiquitin in the $Atg7^{F/+}$:Mx1 (A) and $Atg7^{F/F}$:Mx1 (B) liver. (C–F) Immunoelectron micrographs of ubiquitin in a representative mutant liver. The high-magnification view shows ubiquitin particles near the lipid dropletlike structure (D–F). Bars, 0.5 μm. (G) Immunoblot analysis of the liver. PNS fractions of the liver at 90 d after injection were immunoblotted with the indicated antibodies. Data shown are representative of three separate experiments.

A growing number of disease-associated proteins have been found to accumulate in aggresome, including huntingtin, parkin, α-synuclein, and peripheral myelin protein 22 (Notterpek et al., 1999; Ciechanover and Brundin, 2003). The aggregation of these proteins is thought to be involved in the pathogenesis of Huntington's disease, Parkinson's disease, and peripheral neu-

ropathies, respectively. Enhanced autophagosome formation is prevalent in most of these diseases (Mizushima et al., 2002), and autophagy has also been considered as a caspase-independent cell death pathway (Xue et al., 1999; Bursch, 2001). Our *Atg7* mutant mice should be useful for examining the role of autophagy in the cell death pathway or in a cellular defense mechanism in the pathogenesis of these diseases.

Materials and methods

Generation of $Atg7^{f/f}$ mice

The targeting vector was constructed by insertion of a *loxP* sequences within introns 13 and 14 of *Atg7* gene. Exon 14 was fused to a cDNA fragment encoded by exons 15, 16, and 17 (aa 1786–2097) and polyA signal sequence was added after the stop codon. Neo resistant gene cassette (*mc1-neo-pA*) was ligated behind the polyA signal sequence followed by the second *loxP* sequence, splicing acceptor site, and exon 14 with stop codon preceding the active site. We electroporated the targeting vector into mouse TT2 ES cells, selected with 200 μg/ml G418 (GIBCO BRL), and then screened for homologous recombinants by PCR and Southern blot analyses. PCR primers were as follows: 5′-TGGCTGCTACTTCTGCAATGATGT-3′, 5′-GAAGGGACTGGCTGCTATTGGGCGAAGTGC-3′, and 5′-TTAGCACAGGGAACAGCGCTCATGG-3′. Southern blot analysis was performed by digestion of genomic DNA with EcoRV and hybridization with the probe shown in Fig. 1 A. Genotyping of mice by PCR was performed using the following two primers: 5′-TGGCTGCTACTTCTGCAATGATGT-3′ and 5′-CAGGACAGAGACCATCAGCTCCAC-3′. Progeny containing the $Atg7^{flox}$ allele were bred with *Zp3*-Cre and *Mx1*-Cre transgenic mice to produce $Atg7^{-/-}$ and $Atg7^{f/f}$:Mx1 mice, respectively. With regard to $Atg7^{f/f}$:Mx1 mice, Cre expression in the liver was induced by i.p. injection of pIpC (Sigma-Aldrich). 300 μl pIpC solution (1 mg/ml in water) was injected three times at 48-h intervals. Mice were housed in specific pathogen-free facilities, and the experimental protocol was approved by the Ethics Review Committee for Animal Experimentation of the Tokyo Metropolitan Institute of Medical Science.

RT-PCR analysis

cDNA was synthesized from 5 μg of DNase I–treated total RNA using the SuperScript First-Strand Synthesis System (GIBCO BRL) and oligo $(dT)_{12\text{-}18}$ primers. Specific primers for each gene were as follows: 5′-ATGCCAGGACACCCTGTGAACTTC-3′ and 5′-ACATCATTGCAGAAGTAGCAGCCA-3′ for Atg7, and 5′-GAGCTGAACGGGAAGCTCAC-3′ and 5′-ACCACCCTGTTGCTGTAGC-3′ for G3PDH.

Immunoblot analysis

The fractions were immunoblotted as described previously (Komatsu et al., 2001). The antibodies for Atg7 (Tanida et al., 1999) and Atg5 (Mizushima et al., 2001) were described previously. The antibodies for ubiquitin (DakoCytomation) and actin (MAB1501R; Chemicon International, Inc.) were purchased. The antibodies against LC3, GABARAP, and GATE-16 were raised in rabbits using their specific peptides as antigens. The antibodies against p112, Mss1, and α5 were provided by K.B. Hendil (August Krogh Institute, University of Copenhagen, Copenhagen, Denmark).

Caesarean delivery and measurement of amino acids

Newborns were delivered by caesarean section at 19.0 d postcoitus and placed in a humidified, thermostat-controlled chamber (30°C). Plasma was fixed in 3% sulphosalicylic acid. Amino acids in the supernatant from plasma samples were measured by an amino acid analyzer (L8500A; Hitachi).

Protein degradation assay

The assay was performed essentially as described previously (Gronostajski and Pardee, 1984). In brief, hepatocytes were plated at 5×10^4 cells/well in collagen-coated 24-well plates and cultured in Williams' E medium with 10% FCS (Williams' E/10% FCS) for 24 h. Cells were incubated with Williams' E/10% FCS containing 0.5 μCi/ml [^{14}C]leucine for 24 h to label long-lived proteins. Cells were washed with Williams' E/10% FCS containing 2 mM of unlabeled leucine and incubated with the medium for 2 h to allow degradation of short-lived proteins and minimize the incorporation of labeled leucine, which was released by proteolysis into protein. The cells were then washed with PBS and incubated at 37°C with Krebs-Ringer bicarbonate medium and Williams' E/10% FCS in the presence or absence of protease inhibitors (5 mM monomethylamine, 10 μg/ml E64d and pepstatin, or 5 μM epoxomicin). After 4 h, aliquots of the medium were taken and a one-tenth volume of 100% trichloroacetic acid was added to each aliquot. The mixtures were centrifuged at 12,000 *g* for 5 min, and the acid-soluble radioactivity was determined using a liquid scintillation counter. At the end of the experiment, the cultures were washed twice with PBS, and 1 ml of cold trichloroacetic acid was added to fix the cell proteins. The fixed cell monolayers were washed with trichloroacetic acid and dissolved in 1 ml of 1 N NaOH at 37°C. Radioactivity in an aliquot of 1 N NaOH was determined by liquid scintillation counting. The percentage of protein degradation was calculated according to published procedures (Gronostajski and Pardee, 1984).

Histological examination

Tissues were dissected, fixed in 4% PFA, paraffin embedded, and sectioned. Sections were stained by Meyer's hematoxylin and eosin. For immunohistochemical analysis, sections were blocked in 5% normal goat serum in PBS containing 0.2% Triton X-100, and then incubated with antiubiquitin antibody (1B3; MBL International Corporation) and Alexa 488–labeled secondary antibody (Molecular Probes). Apoptotic cells were detected by TUNEL assay using Apoptag kit (Intergen Company) as described previously (Tateishi et al., 2001). For GFP-LC3 observations, tissues were fixed with 4% PFA, and the cryosections were imaged with a conventional fluorescence microscope. For LC3 staining, hepatocytes were fixed and stained with anti-LC3 antibody as described previously (Kabeya et al., 2000). All fluorescence images were obtained using a fluorescence microscope (model Q550FV; Leica) equipped with cooled charge-coupled device camera (model CTR MIC; Leica). Pictures were taken using Qfluoro software (Leica).

EM and immunoelectron microscopy

Livers were fixed by cardiac perfusion using 0.1 M phosphate buffer containing 2% PFA and 2% glutaraldehyde for conventional EM. They were post-fixed with 1% OsO_4, embedded in Epon812, and sectioned. Immunoelectron microscopy was performed on cryothin sections as described previously (Waguri et al., 1995). In brief, livers were frozen in phosphate buffer with 2.3 M sucrose and 20% polyvinyl pyrrhoridon. Ultrathin sections were mounted on Formvar carbon-coated nickel grids, blocked with 1% BSA in PBS, and incubated with antiubiquitin antibody (1B3) and colloidal gold conjugated secondary antibody.

Other procedures

MEFs were prepared as described previously (Murata et al., 2001). Primary hepatocytes were prepared as described previously (Ueno et al., 1990). Cell starvation was conducted by incubating the cells in Hanks' balanced solution after three separate washes. The SDH activity was assayed as described previously (Ueno et al., 1990).

On line supplemental material

Fig. S1 shows the histological analyses of tissues from $Atg7^{+/-}$ and $Atg7^{-/-}$ mice at 1 d after birth. Fig. S2 shows the loss of Atg7 protein and activity in $Atg7^{f/f}$:Mx1 mouse liver. Fig. S3 shows the histological analyses of tissues from $Atg7^{f/+}$:Mx1 and $Atg7^{f/f}$:Mx1 mice. Fig. S4 shows the cell death in autophagy-deficient liver. Fig. S5 shows the accumulation of ubiquitin-positive inclusions at early stage of autophagy deficiency. Further comments on the data can be found in the legends. Online supplemental material is available at http://www.jcb.org/cgi/content/full/jcb.200412022/DC1.

We thank T. Kaneko, T. Kouno, and K. Tatsumi for technical assistance. We also thank F. Kaji for his help in EM study; A. Kuma for technical guidance in caesarean delivery; K. Tateishi and H. Uozaki for discussion of liver pathology; and T. Fujimura and K. Murayama for amino acid measurements.

This work was supported in part by Grants-in-Aid from the Ministry of Education, Culture, Sports, Science and Technology of Japan.

Submitted: 3 December 2004
Accepted: 22 March 2005

References

Baumeister, W., J. Walz, F. Zuhl, and E. Seemuller. 1998. The proteasome: paradigm of a self-compartmentalizing protease. *Cell.* 92:367–380.

Bence, N.F., R.M. Sampat, and R.R. Kopito. 2001. Impairment of the ubiquitin-proteasome system by protein aggregation. *Science.* 292:1552–1555.

Bursch, W. 2001. The autophagosomal-lysosomal compartment in programmed cell death. *Cell Death Differ.* 8:569–581.

Ciechanover, A., and P. Brundin. 2003. The ubiquitin proteasome system in neurodegenerative diseases: sometimes the chicken, sometimes the egg. *Neuron.* 40:427–446.

Dunn, W.A., Jr. 1994. Autophagy and related mechanisms of lysosome-mediated protein degradation. *Trends Cell Biol.* 4:139–143.

Goldberg, A.L. 2003. Protein degradation and protection against misfolded or damaged proteins. *Nature.* 426:895–899.

Gronostajski, R.M., and A.B. Pardee. 1984. Protein degradation in 3T3 cells and tumorigenic transformed 3T3 cells. *J. Cell. Physiol.* 119:127–132.

Hanaoka, H., T. Noda, Y. Shirano, T. Kato, H. Hayashi, D. Shibata, S. Tabata, and Y. Ohsumi. 2002. Leaf senescence and starvation-induced chlorosis are accelerated by the disruption of an *Arabidopsis* autophagy gene. *Plant Physiol.* 129:1181–1193.

Ichimura, Y., T. Kirisako, T. Takao, Y. Satomi, Y. Shimonishi, N. Ishihara, N. Mizushima, I. Tanida, E. Kominami, M. Ohsumi, et al. 2000. A ubiquitin-like system mediates protein lipidation. *Nature.* 408:488–492.

Kabeya, Y., N. Mizushima, T. Ueno, A. Yamamoto, T. Kirisako, T. Noda, E. Kominami, Y. Ohsumi, and T. Yoshimori. 2000. LC3, a mammalian homologue of yeast Apg8p, is localized in autophagosome membranes after processing. *EMBO J.* 19:5720–5728.

Kabeya, Y., N. Mizushima, A. Yamamoto, S. Oshitani-Okamoto, Y. Ohsumi, and T. Yoshimori. 2004. LC3, GABARAP and GATE16 localize to autophagosomal membrane depending on form-II formation. *J. Cell Sci.* 117:2805–2812.

Klionsky, D.J., and S.D. Emr. 2000. Autophagy as a regulated pathway of cellular degradation. *Science.* 290:1717–1721.

Komatsu, M., I. Tanida, T. Ueno, M. Ohsumi, Y. Ohsumi, and E. Kominami. 2001. The C-terminal region of an Apg7p/Cvt2p is required for homodimerization and is essential for its E1 activity and E1-E2 complex formation. *J. Biol. Chem.* 276:9846–9854.

Kopito, R.R. 2000. Aggresomes, inclusion bodies and protein aggregation. *Trends Cell Biol.* 10:524–530.

Kuhn, R., F. Schwenk, M. Aguet, and K. Rajewsky. 1995. Inducible gene targeting in mice. *Science.* 269:1427–1429.

Kuma, A., M. Hatano, M. Matsui, A. Yamamoto, H. Nakaya, T. Yoshimori, Y. Ohsumi, T. Tokuhisa, and N. Mizushima. 2004. The role of autophagy during the early neonatal starvation period. *Nature.* 432:1032–1036.

Levine, B., and D.J. Klionsky. 2004. Development by self-digestion: molecular mechanisms and biological functions of autophagy. *Dev. Cell.* 6:463–477.

Lewandoski, M., K.M. Wassarman, and G.R. Martin. 1997. Zp3-cre, a transgenic mouse line for the activation or inactivation of loxP-flanked target genes specifically in the female germ line. *Curr. Biol.* 7:148–151.

Liang, X.H., S. Jackson, M. Seaman, K. Brown, B. Kempkes, H. Hibshoosh, and B. Levine. 1999. Induction of autophagy and inhibition of tumorigenesis by beclin 1. *Nature.* 402:672–676.

Massey, A., R. Kiffin, and A.M. Cuervo. 2004. Pathophysiology of chaperone-mediated autophagy. *Int. J. Biochem. Cell Biol.* 36:2420–2434.

Mizushima, N., T. Noda, T. Yoshimori, Y. Tanaka, T. Ishii, M.D. George, D.J. Klionsky, M. Ohsumi, and Y. Ohsumi. 1998. A protein conjugation system essential for autophagy. *Nature.* 395:395–398.

Mizushima, N., A. Yamamoto, M. Hatano, Y. Kobayashi, Y. Kabeya, K. Suzuki, T. Tokuhisa, Y. Ohsumi, and T. Yoshimori. 2001. Dissection of autophagosome formation using Apg5-deficient mouse embryonic stem cells. *J. Cell Biol.* 152:657–668.

Mizushima, N., Y. Ohsumi, and T. Yoshimori. 2002. Autophagosome formation in mammalian cells. *Cell Struct. Funct.* 27:421–429.

Mizushima, N., A. Yamamoto, M. Matsui, T. Yoshimori, and Y. Ohsumi. 2004. In vivo analysis of autophagy in response to nutrient starvation using transgenic mice expressing a fluorescent autophagosome marker. *Mol. Biol. Cell.* 15:1101–1111.

Mortimore, G.E., and A.R. Poso. 1987. Intracellular protein catabolism and its control during nutrient deprivation and supply. *Annu. Rev. Nutr.* 7:539–564.

Murata, S., H. Udono, N. Tanahashi, N. Hamada, K. Watanabe, K. Adachi, T. Yamano, K. Yui, N. Kobayashi, M. Kasahara, et al. 2001. Immunoproteasome assembly and antigen presentation in mice lacking both PA28alpha and PA28beta. *EMBO J.* 20:5898–5907.

Nakagawa, I., A. Amano, N. Mizushima, A. Yamamoto, H. Yamaguchi, T. Kamimoto, A. Nara, J. Funao, M. Nakata, K. Tsuda, et al. 2004. Autophagy defends cells against invading group *A Streptococcus. Science.* 306:1037–1040.

Nishino, I., J. Fu, K. Tanji, T. Yamada, S. Shimojo, T. Koori, M. Mora, J.E. Riggs, S.J. Oh, Y. Koga, et al. 2000. Primary LAMP-2 deficiency causes X-linked vacuolar cardiomyopathy and myopathy (Danon disease). *Nature.* 406:906–910.

Notterpek, L., M.C. Ryan, A.R. Tobler, and E.M. Shooter. 1999. PMP22 accumulation in aggresomes: implications for CMT1A pathology. *Neurobiol. Dis.* 6:450–460.

Ohsumi, Y. 2001. Molecular dissection of autophagy: two ubiquitin-like systems. *Nat. Rev. Mol. Cell Biol.* 2:211–216.

Perlmutter, D.H. 2002. Liver injury in alpha1-antitrypsin deficiency: an aggregated protein induces mitochondrial injury. *J. Clin. Invest.* 110:1579–1583.

Qu, X., J. Yu, G. Bhagat, N. Furuya, H. Hibshoosh, A. Troxel, J. Rosen, E.L. Eskelinen, N. Mizushima, Y. Ohsumi, et al. 2003. Promotion of tumorigenesis by heterozygous disruption of the beclin 1 autophagy gene. *J. Clin. Invest.* 112:1809–1820.

Seglen, P.O., and P. Bohley. 1992. Autophagy and other vacuolar protein degradation mechanisms. *Experientia.* 48:158–172.

Shintani, T., and D.J. Klionsky. 2004. Autophagy in health and disease: a double-edged sword. *Science.* 306:990–995.

Shintani, T., N. Mizushima, Y. Ogawa, A. Matsuura, T. Noda, and Y. Ohsumi. 1999. Apg10p, a novel protein-conjugating enzyme essential for autophagy in yeast. *EMBO J.* 18:5234–5241.

Sutovsky, P., R.D. Moreno, J. Ramalho-Santos, T. Dominko, C. Simerly, and G. Schatten. 1999. Ubiquitin tag for sperm mitochondria. *Nature.* 402:371–372.

Tanaka, Y., G. Guhde, A. Suter, E.L. Eskelinen, D. Hartmann, R. Lullmann-Rauch, P.M. Janssen, J. Blanz, K. von Figura, and P. Saftig. 2000. Accumulation of autophagic vacuoles and cardiomyopathy in LAMP-2-deficient mice. *Nature.* 406:902–906.

Tanida, I., N. Mizushima, M. Kiyooka, M. Ohsumi, T. Ueno, Y. Ohsumi, and E. Kominami. 1999. Apg7p/Cvt2p: a novel protein-activating enzyme essential for autophagy. *Mol. Biol. Cell.* 10:1367–1379.

Tanida, I., E. Tanida-Miyake, T. Ueno, and E. Kominami. 2001. The human homolog of *Saccharomyces cerevisiae* Apg7p is a protein-activating enzyme for multiple substrates including human Apg12p, GATE-16, GABARAP, and MAP-LC3. *J. Biol. Chem.* 276:1701–1706.

Tateishi, K., M. Omata, K. Tanaka, and T. Chiba. 2001. The NEDD8 system is essential for cell cycle progression and morphogenetic pathway in mice. *J. Cell Biol.* 155:571–579.

Tsukada, M., and Y. Ohsumi. 1993. Isolation and characterization of autophagy-defective mutants of *Saccharomyces cerevisiae. FEBS Lett.* 333:169–174.

Ueno, T., S. Watanabe, M. Hirose, T. Namihisa, and E. Kominami. 1990. Phalloidin-induced accumulation of myosin in rat hepatocytes is caused by suppression of autolysosome formation. *Eur. J. Biochem.* 190:63–69.

Waguri, S., N. Sato, T. Watanabe, K. Ishidoh, E. Kominami, K. Sato, and Y. Uchiyama. 1995. Cysteine proteinases in GH4C1 cells, a rat pituitary tumor cell line, are secreted by the constitutive and regulated secretory pathways. *Eur. J. Cell Biol.* 67:308–318.

Xue, L., G.C. Fletcher, and A.M. Tolkovsky. 1999. Autophagy is activated by apoptotic signalling in sympathetic neurons: an alternative mechanism of death execution. *Mol. Cell. Neurosci.* 14:180–198.

Yue, Z., S. Jin, C. Yang, A.J. Levine, and N. Heintz. 2003. Beclin 1, an autophagy gene essential for early embryonic development, is a haploinsufficient tumor suppressor. *Proc. Natl. Acad. Sci. USA.* 100:15077–15082.

Available online at www.sciencedirect.com
SCIENCE DIRECT®
Biochemical and Biophysical Research Communications 331 (2005) 309–317
BBRC
www.elsevier.com/locate/ybbrc

Phosphorylated IκBα is a component of Lewy body of Parkinson's disease

Kazuyuki Noda [a], Toshiaki Kitami [a], Wei Ping Gai [c], Fariba Chegini [c], Poul Henning Jensen [d], Tsutomu Fujimura [b], Kimie Murayama [b], Keiji Tanaka [e], Yoshikuni Mizuno [a], Nobutaka Hattori [a,*]

[a] *Department of Neurology, Juntendo University School of Medicine, 2-1-1 Hongo, Bunkyo-ku, Tokyo 113-8421, Japan*
[b] *Division of Biochemical Analysis, Juntendo University School of Medicine, 2-1-1 Hongo, Bunkyo-ku, Tokyo 113-8421, Japan*
[c] *Department of Human Physiology and Center for Neuroscience, Flinders University, Bedford Park, SA5042, Australia*
[d] *Institute of Medical Biochemistry, University of Aarhus, DK-8000 Aarhus C, Denmark*
[e] *Department of Molecular Oncology, Tokyo Metropolitan Institute of Medical Science, 3-18-22 Honkomagome, Bunkyo-ku, Tokyo 113-8613, Japan*

Received 20 March 2005
Available online 2 April 2005

Abstract

Ubiquitin is one of the major components of Lewy bodies (LB), the pathological hallmark of Parkinson's disease (PD). Here, we identified that a phosphorylated form of IκBα (pIκBα), an inhibitor of NF-κB, and $SCF^{\beta\text{-}TrCP}$, the ubiquitin ligase of pIκBα, are components of LB in brains of PD patients. In vitro studies identified those proteins in the ubiquitin- and α-synuclein (known as the major component of LB)-positive LB-like inclusions generated in dopaminergic SH-SY5Y cells treated with MG132, a proteasome inhibitor. Intriguingly, IκBα migration into such ubiquitinated inclusions in cells treated with MG132 was inhibited by a cell-permeable peptide known to block phosphorylation of IκBα, although this peptide did not influence cell viability under proteasomal inhibition. Our results indicate that phosphorylation of IκBα plays a role in the formation of IκBα-containing inclusions caused by proteasomal dysfunction, and that the generation of such inclusion is independent of cell death caused by impairment of proteasome.

Keywords: Parkinson's disease; Lewy bodies; Ubiquitin; Proteasome; IκBα; IκB-kinase

Parkinson's disease (PD) is one of the most common neurodegenerative disorders among the aged and its pathological hallmark is the preferential degeneration of dopaminergic neurons in the substantia nigra (SN) and the appearance of intracytoplasmic inclusions known as Lewy bodies (LB). The process of LB formation could provide important clues regarding the pathogenesis of PD because important proteins, such as α-synuclein (another familial PD gene product) and ubiquitin (Ub), are components of these inclusions [1,2].

The ubiquitin–proteasome pathway (UPP) is the major non-lysosomal degradation system for various proteins, such as short-lived, misfolded, and damaged polypeptides [3]. In this system, ubiquitin is conjugated to lysine residue of the target protein by a cascade of enzymatic reactions catalyzed by the E1 (Ub-activating), E2 (Ub-conjugating), and E3 (Ub-ligating) enzymes in an ATP-dependent manner, and polyubiquitination marks the proteins for degradation by the proteasome. Several lines of evidence suggest that derangements in the UPP play an important role in the pathogenesis of PD and describe inhibited hydrolytic activities of the proteasome in PD [4,5].

* Corresponding author. Fax: +81 3 5800 0547.
E-mail address: nhattori@med.juntendo.ac.jp (N. Hattori).

0006-291X/$ - see front matter © 2005 Elsevier Inc. All rights reserved.
doi:10.1016/j.bbrc.2005.03.167

On the other hand, the concentration of tumor necrosis factor-α (TNF-α), a proinflammatory cytokine, is increased in PD and this cytokine plays a role in the pathogenesis of PD [6,7]. TNF-α stimulates the multisubunit IκB-kinase (IKK), which is composed of IKKα, IKKβ and a non-catalytic regulatory component named NF-κB essential modifier (NEMO), which allows IκBα to be subsequently phosphorylated. The phosphorylated form, pIκBα, is polyubiquitinated by the $SCF^{\beta\text{-}TrCP}$ ubiquitin ligase [8–10]. Subsequently, they are rapidly degraded by 26S proteasomes, and NF-κB enters the nucleus, binds to DNA, and activates transcription of target genes [11]. In this scenario, the nuclear translocation of NF-κB is masked by physical association with IκBα, resulting in retention of NF-κB in the cytoplasm.

Intriguingly, a previous report implicated the involvement of NF-κB in the LB of PD [12], but the role of IκBα in the pathogenesis of PD remains unclear. The aims of the present study were the following: (1) to determine the presence or absence of pIκBα and components of the $SCF^{\beta\text{-}TrCP}$ complex in LB of PD, (2) whether pIκBα is colocalized in the cytoplasmic inclusions formed in MG132-treated human dopaminergic neuroblastoma cells (SH-SY5Y), and (3) to determine the effect of inhibition of IκBα phosphorylation on the formation of cytoplasmic inclusions and viability of cells treated with a proteasome inhibitor.

Materials and methods

Human neuroblastoma cell lines. Human dopaminergic neuroblastoma SH-SY5Y cells were cultured in Dulbecco's modified Eagle's medium (DMEM) containing 10%(v/v) fetal bovine serum and penicillin/streptomycin at 37 °C in a humidified 5% CO_2 atmosphere. To induce differentiation, the cells were treated with 10 μM retinoic acid (Sigma Chemical, St. Louis, MO) in the dark for 4–6 days as described previously [13–15].

Application of agents. TNF-α (R&D Systems, Minneapolis, MN) and MG132 (Peptide Institute, Osaka, Japan) were prepared at 10 μg/ml (in H_2O) and 10 mM (in dimethyl sulfoxide, DMSO) stock solutions, respectively. The specific antibodies used were rabbit anti-ubiquitin (Dako, Carpinteria, CA), mouse anti-ubiquitin 1510 (Chemicon International, Temecula, CA), anti-synuclein-1 (Transduction Laboratories, Lexington, KY), sheep anti-α-synuclein [16], anti-pIκBα (Ser32), and anti-IκBα antibodies (from Cell Signaling Technology, Beverly, MA, and Calbiochem, La Jolla, CA). Anti-NF-κB p65 (sc-372) and anti-β-TrCP (N-15) antibodies were purchased from Santa Cruz Biotechnology (Santa Cruz, CA). Note that anti-IκBα antibody reacts with both phosphorylated and unphosphorylated forms of IκBα. Anti-ROC1 and Cul-1 antibodies were prepared as described previously [17]. The secondary antibodies used were goat anti-mouse IgG coupled with Alexa Fluor 488, goat anti-mouse IgG coupled with Alexa Fluor 594, anti-rabbit IgG coupled with Alexa Fluor 594 (Molecular Probes, Eugene, OR), and fluorescein goat anti-rabbit IgG (Vector Laboratories, Burlingame, CA).

Immunohistochemistry. For the LB staining experiments using paraffin embedded samples, autopsied brains from seven patients with PD (age, 51–78 years), one patient with dementia with Lewy bodies (DLB, age, 64 years), and five control subjects (age, 20–65 years) were examined. The five control samples were obtained from patients free of neurological diseases and confirmed to have no neuropathological changes in sections of the substantia nigra pars compacta. Immunohistochemistry was performed as described previously [18].

Immunolabeling of isolated Lewy bodies. Immunomagnetic isolation and immunostaining of LB and Lewy neuritis from fresh frozen brains of patients with DLB were performed as described previously [19]. Smears were prepared on gelatin-coated glass slides, from homogenates, factions of each washing step, and LB-enriched Percoll fractions. The smears were air-dried overnight, fixed for 10 min in 4% formaldehyde–2% picric acid–0.1 M phosphate-buffered saline (pH 7.4), and then incubated for 10 min in 3% H_2O_2 in 50% methanol in Tris-buffered saline (TBS, pH 7.4). Following three rinses in 0.1 M TBS containing 0.05% sodium azide and 1 mM phenylmethylsulfonyl fluoride (PMSF) (TBS), the smears were incubated with 20% normal horse serum in TBS for 30 min to block non-specific antibody-binding sites, and incubated overnight with sheep antibody against α-synuclein and pIκBα, ROC1, Cul-1, and β-TrCP in TBS containing 0.5% bovine serum albumin. Control sections were stained by incubating the smears with TBS containing either or neither antibodies. Following three rinses in TBS, the smears were incubated for 1 h with donkey anti-sheep IgG or donkey anti-rabbit IgG conjugated with Cy2, Cy3 or Cy5 in TBS (all from Jackson Immunoresearch Laboratories, West Grove, PA), with the fluorochromes either singly or in combinations of Cy2/Cy3 or Cy2/Cy5.

Immunocytochemistry. For double-labeling immunofluorescence staining, fixed cells were permeabilized with 0.25% Triton X-100 for 20 min. The cells were blocked with 5% normal goat serum for 1 h, followed by incubation of antibodies to ubiquitin (Chemicon; diluted 1:100), pIκBα Ser32 (Cell Signaling; diluted 1:100), ROC1 (diluted 1:100), or Cullin-1 (diluted 1:100) for 1 h at room temperature. After washing in TBS, the cells were incubated in anti-mouse, anti-rabbit fluorochrome-linked secondary antibodies. After washing in TBS, the cells were covered with glass slides using mounting medium with 4′,6′-diamidine-2-phenylindole dihydrochloride (DAPI) to visualize cell nuclei (Vector Laboratories). To assess the colocalization of ubiquitin and α-synuclein, we used anti-ubiquitin (Dako; diluted 1:100) and anti-synuclein-1 (diluted 1:100) antibodies. Signal was observed under a Zeiss LSM 510 laser-scanning confocal microscope (Zeiss, NY).

Western blotting. Neuronally differentiated SH-SY5Y cells were treated for 24 h with 10 μM MG132 or 20 ng/ml TNF-α. The cells were simultaneously preincubated for 2 h with 10 μM MG132, followed by treatment for 22 h with 10 μM MG132 in the presence of 20 ng/ml TNF-α. The cells were collected and washed in ice-cold phosphate-buffered saline (PBS) and lysis buffer as described previously [20]. Detergent-insoluble material was pelleted by centrifugation at 100,000*g* for 20 min and resuspended in 50 mM Tris–HCl (pH 7.4) and 6 M urea. Equal amounts of protein from both fractions were separated by sodium dodecyl sulfate–polyacrylamide gel electrophoresis (SDS–PAGE) (10% or 10–20%) and transferred onto polyvinylidene difluoride (PVDF) membranes, blocked in 5% non-fat milk for 1 h at room temperature, and incubated at 4 °C with specific antibodies.

Treatment of IKK inhibiting peptide. Recent studies have reported that an NH_2-terminal α-helical region of NEMO associates with a hexapeptide sequence within the extreme carboxyl terminus of IKKβ and IKKα, termed NEMO-binding domain (NBD). Importantly, a short cell-permeable peptide spanning the IKKβ NBD was found to disrupt the association of NEMO with IKKβ and blocked the activity of IKK [21]. We synthesized two peptides at Juntendo University School of Medicine, a functional wild-type NBD with a sequence derived from the Antennapedia homeodomain that mediates membrane translocation without loss of cell viability, and a negative control mutant NBD, as described previously [21–24]. To determine how inhibition of phosphorylation of IκBα affects the formation of such inclusions, the differentiated SH-SY5Y cells were preincubated for 3 h with 40 μM of either wild-type or mutant NBD peptide, followed by treatment for 24 h with 10 μM MG132 in the presence of 40 μM of each NBD peptide. The cells were simultaneously preincubated for 3 h

with no peptide, followed by treatment for 24 h with 10 μM MG132 alone. These cells with ubiquitin-positive inclusions were co-stained with antibodies against pIκBα or IκBα.

Cell viability assay. Cell viability assay was performed using 2-(2-methoxy-4-nitrophenyl)-3-(4-nitrophenyl)-5-(2,4-disulfophenyl)-2H-tetrazolium monosodium salt assay, as described previously [25]. The differentiated SH-SY5Y cells were plated on a 96-well plate and incubated for 24 h at 37 °C in 5% CO_2. The cells were preincubated for 3 h with 40 μM of either wild-type or mutant NBD peptide, followed by treatment for 24 h with 40 μM of each NBD peptide in the presence or absence of 10 μM MG132. The cells were simultaneously preincubated for 3 h with no peptide, followed by treatment for 24 h with 10 μM MG132 alone. The live cell count was assayed using Cell Counting Kit-8 according to the instructions provided by Doujin (Cell Counting Kit-8; Kumamoto, Japan).

Statistical analysis. All data are expressed as means ± SEM. Comparisons between groups were performed using analysis of variance (Tukey's multiple *t* test).

A p value <0.05 indicated statistically significant differences.

Results

Phosphorylated IκBα and $SCF^{\beta\text{-}TrCP}$ complex are novel components of Lewy bodies

We first examined whether LB contain pIκBα and the components of $SCF^{\beta\text{-}TrCP}$ complex, which are major downstream components of the TNF-α signaling pathway. Immunohistochemical analysis revealed that anti-pIκBα and ROC1 antibodies predominantly recognized the LB in PD cases (Figs. 1A and B). Immunostaining with anti-NF-κB p65 antibody also showed the staining of LB (Fig. 1C). Anti-pIκBα and anti-ROC1 signals were strongly present in the halo region of LB, and the anti-NF-κB-p65 signal was present in the core region. In contrast, such immunoreactivities for pIκBα ROC1 and NF-κB were not observed in the control brains and when the primary antibody was omitted in PD and DLB brains (data not shown).

In the next step, the isolated LB were used to investigate whether these proteins are associated with LB. Confocal laser-scanning microscopic examination of sections prepared from freshly isolated LB from postmortem brains of DLB showed immunoreactivities for pIκBα, ROC1, Cul-1, and β-TrCP (Figs. 1D, G, J, and M). LB were identifiable by their strong α-synuclein staining in smears of isolated LB from DLB cortex (Figs. 1E, H, K, and N), but not in sections from a normal control cortex (data not shown). These immunoreactivities for the indicated antibodies in LB were distributed across or sometimes more concentrated in the central region of LB (Figs. 1F, I, L, and O). Counting of α-synuclein-positive LB indicated that 80–90% of the cortical LB ($n = 300$, pooled from three DLB cases) were also positive for ROC1 and Cul-1. A similar staining pattern was also observed in LB isolated from the substantia nigra (SN) of PD (data not shown).

Localization of pIκBα, ROC1, and Cul-1 in cytoplasmic inclusions of SH-SY5Y cells

As a model for the formation of cytoplasmic inclusions, we used SH-SY5Y cell lines treated with MG132 [26]. Localization of pIκBα, ROC1, and Cul-1 was investigated after the addition of 10 μM MG132 for 24 h in differentiated SH-SY5Y cells. Proteasomal dysfunction caused typical cytoplasmic inclusions that were stained with anti-ubiquitin (Ub) antibodies, and interestingly many, if not all, ubiquitinated inclusions were also positive for pIκBα, ROC1, and Cul-1 (Figs. 2A–C). Under normal conditions without MG132, the cells displayed low-level cytoplasmic staining for the indicated proteins (data not shown). Although we examined the effect of TNF-α on the formation of the inclusions, no inclusions that contained ubiquitin and pIκBα were observed after treatment with TNF-α alone. In addition, the effect of simultaneous treatment with TNF-α and MG132 was not significantly different from the results of MG132 treatment alone (data not shown).

We next examined whether these cells also contained α-synuclein in such cytoplasmic ubiquitinated inclusions. Following proteasomal inhibition with 10 μM MG132, some of the ubiquitinated cytoplasmic inclusions also exhibited α-synuclein immunoreactivity (Fig. 2D). Moreover, we examined whether pIκBα and components of the SCF complex colocalize with α-synuclein in the presence of 10 μM MG132. The α-synuclein-positive inclusions were also immunoreactive for pIκBα ROC1 and Cul-1 following treatment with 10 μM MG132 (Figs. 2E–G). The proportion of cells treated with 10 μM MG132 that contained aggregates immunoreactive for both pIκBα and α-synuclein was 7.98 ± 1.14%. In contrast, the proportion of 10 μM MG132-treated cells containing inclusions positive for both pIκBα and ubiquitin was 23.19 ± 3.84%, suggesting the relative low frequency of α-synuclein/pIκBα-containing inclusions (see Fig. 5B). Inclusions containing only ubiquitin, α-synuclein, or pIκBα were also noted, and their size was also comparatively heterogeneous (data not shown).

Inhibition of proteasomes increases phosphorylated IκBα level in SH-SY5Y cells

We examined the migration pattern of endogenous ubiquitin or pIκBα by SDS–PAGE in differentiated SH-SY5Y cells following proteasomal inhibition with MG132 and/or TNF-α for 24 h. Cells were treated as indicated in Fig. 3, and then the resulting cell extracts were separated into detergent-soluble and detergent-insoluble fractions. Treatment with 10 μM MG132 resulted in accumulation of high-molecular weight ubiquitin–protein conjugates particularly within the insoluble fractions but not in TNF-α alone and control

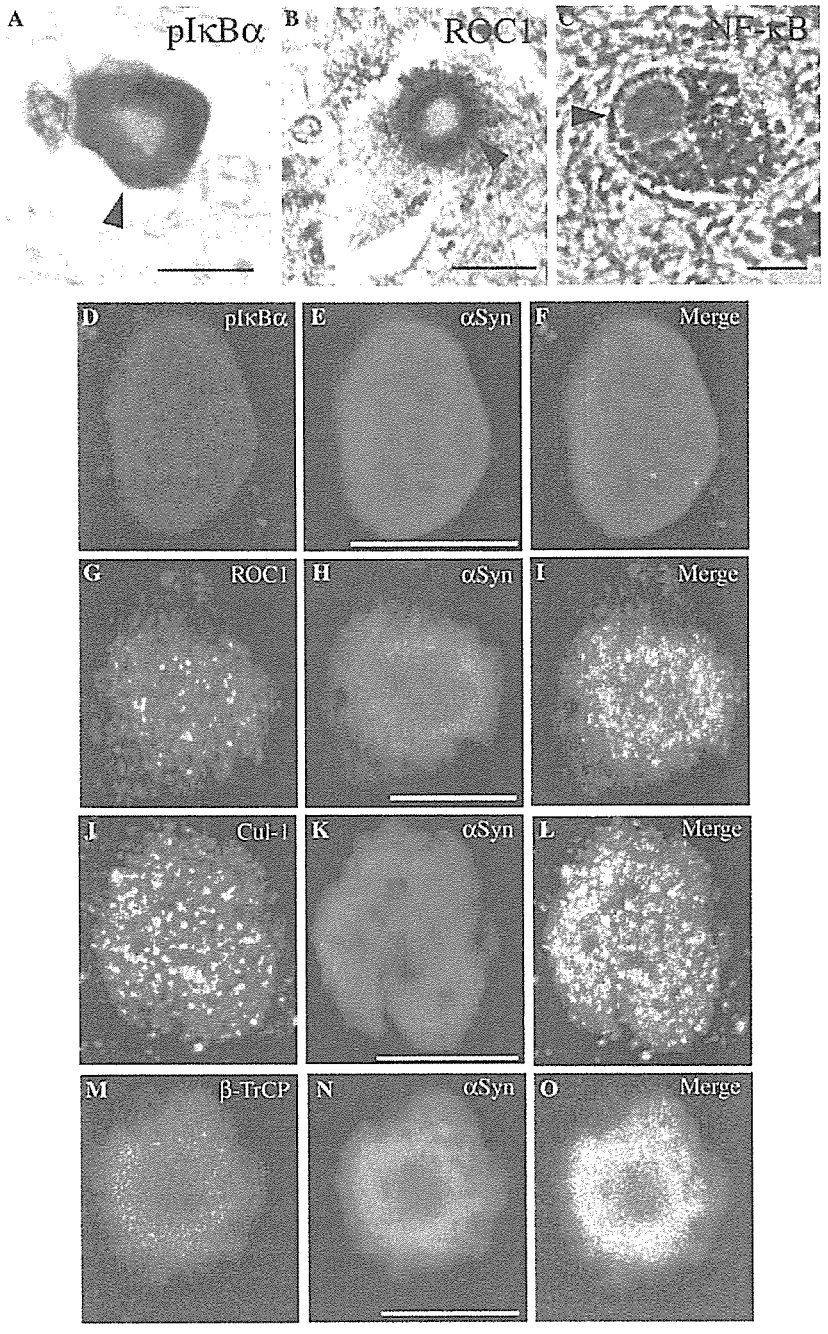

Fig. 1. Identification of phosphorylated IκBα and components of $SCF^{\beta\text{-}TrCP}$ in Lewy bodies. (Upper panel) Paraffin sections of autopsied human brain samples with PD were immunostained with antibodies against pIκBα (A), ROC1 (B), and NF-κB p65 (C). Lewy bodies are marked by arrowheads. Scale bars = 20 μm (A–C). (Lower panel) Colocalization of α-synuclein (αSyn), pIκBα, and components of $SCF^{\beta\text{-}TrCP}$ in isolated LB from DLB (Dementia with LB) cases. LB were identified by α-synuclein staining. Each preparation was doubly stained with sheep anti-α-synuclein (E, H, K, and N) and various antibodies against pIκBα (D), ROC1 (G), Cul-1 (J), and β-TrCP (M), and analyzed with a laser-scanning confocal microscope. Panels (F, I, L, and O) at right correspond to merged images; yellow-colored structures indicate colocalization. Scale bars = 10 μm (D–O).

cells (Fig. 3A). Unexpectedly, the effect of TNF-α was very weak in SH-SY5Y cells, because no massive reduction of IκBα was observed upon treatment with TNF-α for 1, 12, or 24 h (Fig. 3C and data not shown). This finding was in marked contrast to the almost complete disappearance of IκBα in HeLa cells treated with 20 ng/ml TNF-α within 1 h (data not shown). However, TNF-α significantly increased the pIκBα level (Fig. 3B), indicating the existence of TNF-α response to a lesser extent in SH-SY5Y cells. It is of note that MG132 alone

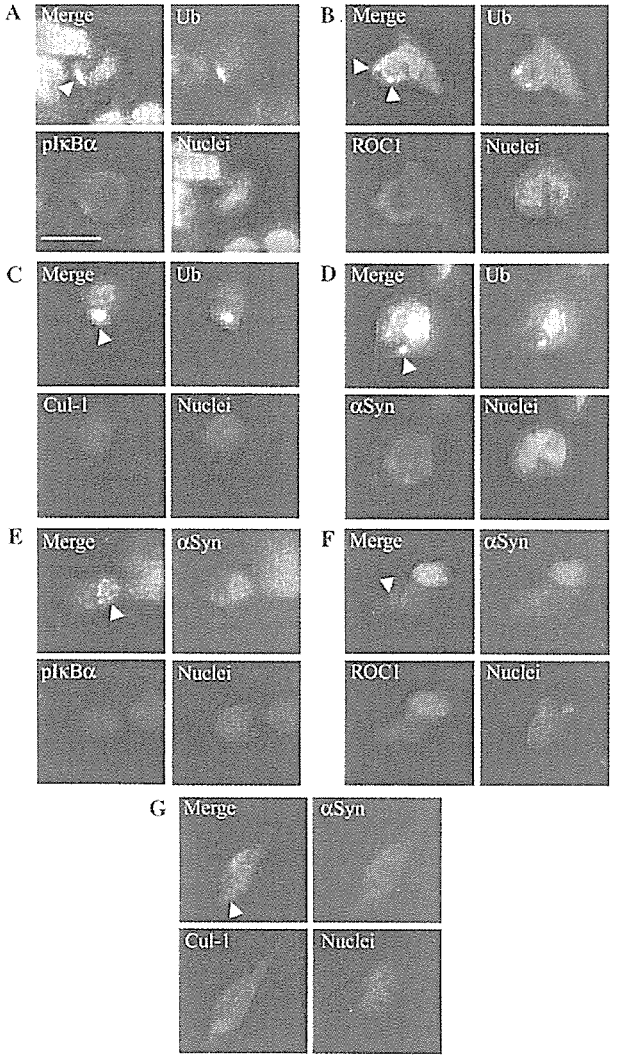

Fig. 2. Proteasomal inhibition leads to formation of pIκBα-positive cytoplasmic inclusions in SH-SY5Y cells. Differentiated SH-SY5Y cells were treated with 10 μM MG132 for 24 h, fixed and then double-stained with various combinations of antibodies as indicated. (A–D) Cytoplasmic inclusions positive for ubiquitin (Ub) were co-stained for pIκBα (A), ROC1 (B), Cul-1 (C), and α-synuclein (D). Arrowheads indicate the inclusions. Regions of overlap between ubiquitin (green) and immunoreactivities of the indicated proteins (red) appear in yellow color. (E–G) α-Synuclein (αSyn)-positive cytoplasmic inclusions were co-stained for pIκBα (E), ROC1 (F), and Cul-1 (G). Regions of overlap between α-synuclein (green) and immunoreactivities of the indicated proteins (red) appear in yellow color. Scale bar = 10 μm.

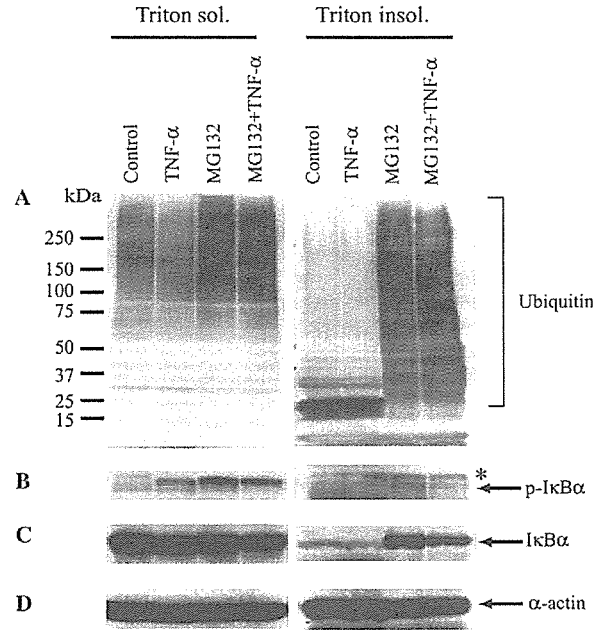

Fig. 3. Inhibition of the proteasome results in accumulation of pIκBα within the detergent-insoluble fraction of SH-SY5Y cells. The cells were treated for 24 h with 10 μM MG132 and/or 20 ng/ml TNF-α, and the cell lysates were processed for Western blotting, as described in Materials and methods. The protein was blotted onto PVDF membranes and probed with antibodies against ubiquitin (A), pIκBα (B), and IκBα (C). Note that anti-IκBα antibody reacted both phosphorylated and unphosphorylated forms. α-Actin served as a loading control (D). Asterisk indicates a non-specific band.

increased the pIκBα level in the cells (Fig. 3B), although additive effects of TNF-α and MG132 were not observed for phosphorylation of IκBα. Intriguingly, when detergent-soluble and -insoluble fractions were immunoblotted with anti-pIκBα or anti-IκBα antibody, both proteins were clearly detected in the detergent-insoluble fraction after treatment with 10 μM MG132 but not in TNF-α alone and control cells (Figs. 3B and C). In addition, simultaneous treatment with TNF-α and MG132 had no significant effects in comparison with MG132 treatment alone. Thus, it is clear that IκBα, perhaps its phosphorylated form, is incorporated into the detergent-insoluble fraction under the conditions of proteasome inhibition.

The NBD peptide inhibits pIκBα entry into cytoplasmic ubiquitin-positive inclusions

The presence of pIκBα in LB of autopsied brains of PD patients and ubiquitinated inclusions in SH-SY5Y in the present study led us to examine whether inhibition of IKK, which phosphorylates IκBα, alters the processes of inclusion formation and cell death. First, we determined the optimal concentration of the cell-permeable NBD peptide, which is known to block the activity of IKK. To study the effect of NBD, SH-SY5Y cells were pre-treated with various concentrations of wild-type NBD for 3 h and then stimulated by 20 ng/ml TNF-α. In the present study, we used 40 μM NBD as the optimal concentration to block phosphorylation of IκBα. We also examined the effect of high concentrations of the NBD peptide (about 1000 μM), as described previously [21], but peptide toxicity was observed in our cell lines.

We next treated the cells with MG132 in the presence or absence of NBD peptide and then performed double

staining using antibodies for pIκBα, IκBα, and ubiquitin. Ubiquitinated inclusions containing pIκBα were identified in cells treated with MG132 alone or with MG132 in the presence of mutant NBD lacking inhibitory activity for IKK. On the other hand, while ubiquitinated inclusions were observed in cells treated with MG132 in the presence of wild-type NBD, only a few cells contained ubiquitinated inclusions positive for pIκBα (Fig. 4A). In addition, the use of an antibody for IκBα in the presence of wild-type NBD was also associated with reduced number of cells with ubiquitinated inclusions positive for IκBα, compared with those treated with MG132 or MG132 in the presence of mutant NBD (Fig. 4B), indicating that phosphorylation of IκBα may be required for its incorporation into cytoplasmic inclusions generated by proteasome inhibition.

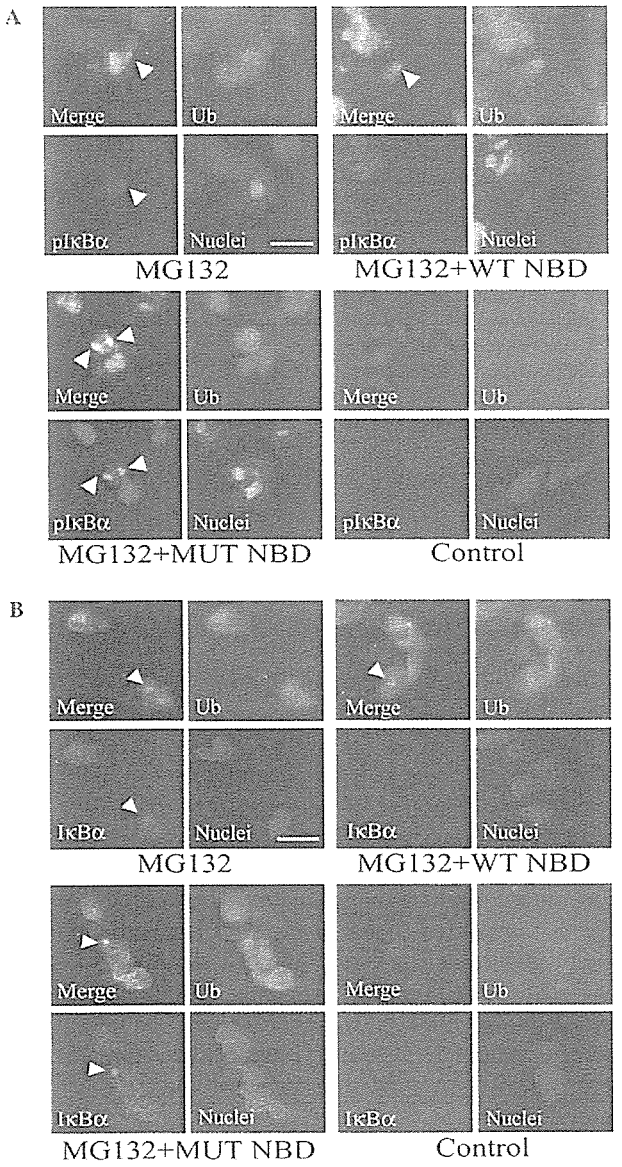

Fig. 4. Wild-type NBD decreases pIκBα level within the ubiquitinated inclusions in SH-SY5Y cells. The cells were treated for 24 h with 10 μM MG132 alone, or with 10 μM MG132 in the presence of 40 μM of either wild-type (WT NBD) or mutant NBD peptide (MUT NBD) as indicated in Materials and methods. Cells with ubiquitinated inclusions were co-stained with pIκBα (A) and IκBα (B). Arrowheads indicate the ubiquitinated inclusions. Regions of overlap between ubiquitin (green) and immunoreactivities of the indicated proteins (red) are shown in yellow color. Scale bar = 20 μm.

We then counted the number of cells with aggregated immunoreactivity for both ubiquitin and pIκBα antibodies under basal condition and following treatment with 10 μM MG132 with or without NBD peptide. It is worth noting that whereas approximately 50% of total cells contained ubiquitin-positive inclusions, pIκBα-positive inclusions were below 25% (Figs. 5A and B), suggesting that pIκBα is not incorporated into all inclusions. Wild-type NBD significantly decreased the number of cells with ubiquitinated inclusions (Fig. 5A, $p < 0.05$), and cells with cytoplasmic inclusions positive for pIκBα and ubiquitin, compared with cells treated with MG132 alone (Fig. 5B, $p < 0.001$). In comparison, mutant NBD did not show the same effects on phosphorylation of IκBα as wild-type NBD. Finally, we examined the toxicity of 10 μM MG132 on these cell lines. Treatment with 10 μM MG132 reduced cell viability to $37.84 \pm 1.46\%$. In contrast, wild-type NBD did not influence cell viability under proteasomal inhibition (Fig. 5C).

Discussion

The appearance of LB in SN is a prominent feature in PD, but the pathogenic role of such inclusions remains elusive. In this study, we identified novel components including pIκBα and components of $SCF^{\beta\text{-}TrCP}$ ligase in LB. To date, several studies have reported that the UPP-related proteins (such as ubiquitin, the 20S proteasome subunit, and HSP70) are localized in LB of PD [27,28]. These findings indicate that there appears to be an important correlation between some pathological alteration in UPP and the formation of LB in PD. In this regard, the pathogenic nature of proteasomal dysfunction has been studied in experimental models using a proteasome inhibitor. It has been demonstrated that inhibition of proteasomal function induces the formation of cytoplasmic inclusions immunoreactive for ubiquitin and α-synuclein in PC12 cells and mesencephalic cultures [20,29]. These observations suggest that proteasomal dysfunction is associated with the development of cytoplasmic inclusions that may have features similar to those of LB, in terms of containing two proteins; i.e., α-synuclein and ubiquitin, described as the major components of LB [2].

pIκBα and SCF ligase are also involved in UPP-related proteins, and these molecules have not been adequately studied in PD. Therefore, to explore how these

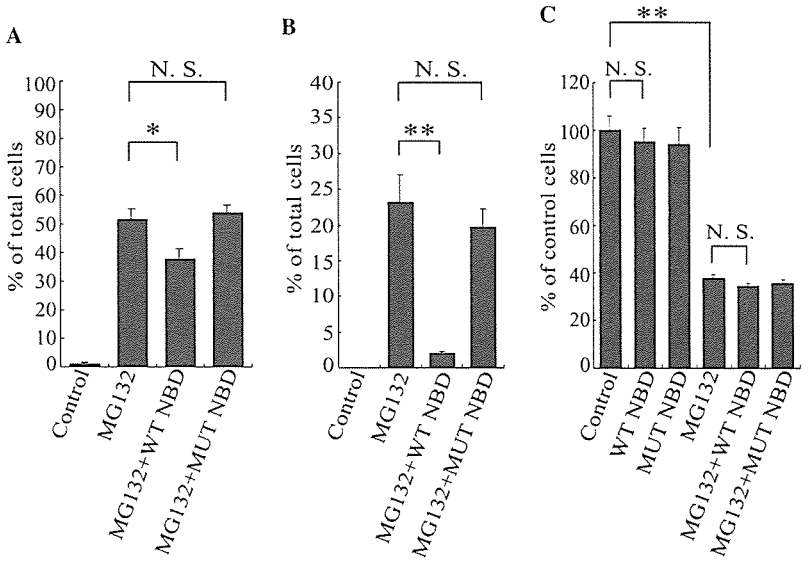

Fig. 5. Effects of NBD on formation of pIκBα-containing inclusions and cell death caused by proteasomal inhibition. After the cells were treated as explained in Fig. 4, the proportions of cells with cytoplasmic inclusions were determined. (A) The proportion of cells with ubiquitin-positive inclusions was calculated relative to total cells. (B) The proportion of cells with ubiquitinated inclusions containing pIκBα was calculated relative to total cells. In each experiment, 10 fields of 50 cells were counted. Similar effects of NBD were seen in two or more independent experiments. Data are means ± SEM. $*p < 0.05$; $**p < 0.001$ for differences between cell lines (Tukey's multiple t test). NS, not significant. (C) Cell viability was assessed as described in Materials and methods, and is expressed as the percentage of untreated cells. Similar results were seen in three independent experiments. Values are means ± SEM, each $n = 8$. $**p < 0.001$ for differences between cell lines (Tukey's multiple t test).

molecules are present in LB would be important in considering the process of LB formation. In our cell culture model, inhibition of normal proteasomal function by MG132 also induced the formation of ubiquitinated cytoplasmic inclusions containing α-synuclein, and this finding is consistent with previous reports [20,29], as described above. Intriguingly, our results showed that these inclusions were positive for pIκBα and some components of its ligase that are found in the LB. These findings suggest that the existence of pIκBα in LB is more likely and proteasomal dysfunction is an important factor in the formation of cytoplasmic inclusions.

Using SDS–PAGE analysis of detergent-soluble and -insoluble fractions, we found high-molecular weight ubiquitinated proteins particularly in the detergent-insoluble fraction, and pIκBα in the insoluble fraction following proteasomal inhibition with MG132. In contrast, after incubation with TNF-α alone, neither high-molecular weight ubiquitinated bands nor pIκBα was detected in the insoluble fractions, and cytoplasmic inclusions containing ubiquitin and pIκBα were not observed. These findings suggest that phosphorylation of IκBα alone is insufficient for the formation of cytoplasmic inclusions, and there appears to be a strong causal link between the accumulation of poorly degraded proteins, resulting from proteasomal dysfunction, and the formation of cytoplasmic inclusions.

We also showed that the presence of pIκBα in the ubiquitinated inclusions was markedly inhibited by a specific IKK inhibitor, under the conditions of MG132 treatment. This finding also supports the above-mentioned data that pIκBα is involved in the cytoplasmic inclusions resulting from proteasomal inhibition in our SH-SY5Y cells. In addition, this finding provides us a further possibility. In some neurodegenerative disorders, the ubiquitin-positive inclusions are considered to involve the ubiquitin–protein conjugates [28,30]. However, it is not clear which types of proteins are directly polyubiquitinated in LB. IκBα is phosphorylated by IKK, and pIκBα is polyubiquitinated by the $SCF^{\beta\text{-}TrCP}$, then degraded by the 26S proteasome. Thus, it is conceivable that once phosphorylation of IκBα is inhibited, neither polyubiquitination after its phosphorylation nor accumulation of IκBα into inclusion bodies is observed. We demonstrated that wild-type NBD peptide reduced the proportion of not only ubiquitin-positive inclusions, but also ubiquitinated inclusions containing pIκBα. Based on our finding, it is possible that the polyubiquitination of pIκBα resulting from proteasomal dysfunction triggers its entry into ubiquitinated cytoplasmic inclusions.

It is still not clear whether LB are cytoprotective or cytotoxic for neurons in the SN of PD. Recent studies suggest that the formation of protein aggregates or intracellular inclusions may be beneficial for cell survival rather than enhance cell death [31,32]. In the present study, exposure to MG132 alone or MG132 in the presence of wild-type NBD peptide did not alter cell viability whereas the same conditions decreased the ubiquitinated cytoplasmic inclusions. This finding at least supports the

conclusion of the above studies [31,32], i.e., the formation of cytoplasmic inclusions is not a toxic response against cell survival. Viewed from a different angle, our finding may suggest that inclusion bodies formed following proteasomal inhibition are independent of cell death.

In conclusion, we demonstrated the presence of pIκBα in LB of PD, and that similar inclusion bodies are produced in the presence of significant proteasomal dysfunction in cultured cells. Our observations in cultured cells may reflect, at least in part, the formation of LB in dopaminergic neurons of PD.

Acknowledgments

The authors thank Drs. Hideo Fujiwara and Takeshi Iwatsubo (University of Tokyo) for providing excellent advice. This study was supported by grants from the Ministry of Education, Science, Sports and Culture of Japan, by the Fund for "Research for the Future" Program from the Japan Society for the Promotion of Science. This study was also supported by funds from the NH&MRC and Michael J Fox Foundation.

References

[1] T. Iwatsubo, H. Yamaguchi, M. Fujimuro, H. Yokosawa, Y. Ihara, J.Q. Trojanowski, V.M. Lee, Purification and characterization of Lewy bodies from the brains of patients with diffuse Lewy body disease, Am. J. Pathol. 148 (1996) 1517–1529.

[2] M.G. Spillantini, M.L. Schmidt, V.M. Lee, J.Q. Trojanowski, R. Jakes, M. Goedert, α-Synuclein in Lewy bodies, Nature 388 (1997) 839–840.

[3] S.J.S. Berke, H.L. Paulson, Protein aggregation and the ubiquitin proteasome pathway: gaining the UPPer hand on neurodegeneration, Curr. Opin. Genet. Dev. 13 (2003) 253–261.

[4] K.S. McNaught, R. Belizaire, O. Isacson, P. Jenner, C.W. Olanow, Altered proteasomal function in sporadic Parkinson's disease, Exp. Neurol. 179 (2003) 38–46.

[5] G.K. Tofaris, A. Razzaq, B. Ghetti, K.S. Lilley, M.G. Spillantini, Ubiquitination of α-synuclein in Lewy bodies is a pathological event not associated with impairment of proteasome function, J. Biol. Chem. 278 (2003) 44405–44411.

[6] G. Boka, P. Anglade, D. Wallach, F. Javoy-Agid, Y. Agid, E.C. Hirsch, Immunocytochemical analysis of tumor necrosis factor and its receptors in Parkinson's disease, Neurosci. Lett. 172 (1994) 151–154.

[7] T. Nagatsu, M. Mogi, H. Ichinose, A. Togari, Changes in cytokines and neurotrophins in Parkinson's disease, J. Neural Transm. Suppl. 60 (2000) 277–290.

[8] H. Suzuki, T. Chiba, T. Suzuki, T. Fujita, T. Ikenoue, M. Omata, K. Furuichi, H. Shikama, K. Tanaka, Homodimer of two F-box proteins βTrCP1 or βTrCP2 binds to IκBα for signal-dependent ubiquitination, J. Biol. Chem. 275 (2000) 2877–2884.

[9] M. Karin, Y. Ben-Neriah, Phosphorylation meets ubiquitination: the control of NF-κB activity, Annu. Rev. Immunol. 18 (2000) 621–663.

[10] P. Strack, M. Caligiuri, M. Pelletier, M. Boisclair, A. Theodoras, P. Beer-Romero, S. Glass, T. Parsons, R.A. Copeland, K.R. Auger, P. Benfield, L. Brizuela, M. Rolfe, SCF(β-TRCP) and phosphorylation dependent ubiquitination of IκBα catalyzed by Ubc3 and Ubc4, Oncogene 19 (2000) 3529–3536.

[11] A.S. Baldwin Jr., The NF-κB and IκB proteins: new discoveries and insights, Annu. Rev. Immunol. 14 (1996) 649–683.

[12] T. Togo, E. Iseki, W. Marui, H. Akiyama, K. Ueda, K. Kosaka, Glial involvement in the degeneration process of Lewy body-bearing neurons and the degradation process of Lewy bodies in brains of dementia with Lewy bodies, J. Neurol. Sci. 184 (2001) 71–75.

[13] J.L. Biedler, S. Roffler-Tarlov, M. Schachner, L.S. Freedman, Multiple neurotransmitter synthesis by human neuroblastoma cell lines and clones, Cancer Res. 38 (1978) 3751–3757.

[14] S.I. Kubo, T. Kitami, S. Noda, H. Shimura, Y. Uchiyama, S. Asakawa, S. Minoshima, N. Shimizu, Y. Mizuno, N. Hattori, Parkin is associated with cellular vesicles, J. Neurochem. 78 (2001) 42–54.

[15] M. Sharma, P. Sharma, H.C. Pant, CDK-5-mediated neurofilament phosphorylation in SHSY5Y human neuroblastoma cells, J. Neurochem. 73 (1999) 79–86.

[16] H. Braak, D. Sandmann-Keil, W. Gai, E. Braak, Extensive axonal Lewy neurites in Parkinson's disease: a novel pathological feature revealed by α-synuclein immunocytochemistry, Neurosci. Lett. 265 (1999) 67–69.

[17] T. Kawakami, T. Chiba, T. Suzuki, K. Iwai, K. Yamanaka, N. Minato, H. Suzuki, N. Shimbara, Y. Hidaka, F. Osaka, M. Omata, K. Tanaka, NEDD8 recruits E2-ubiquitin to SCF E3 ligase, EMBO J. 20 (2001) 4003–4012.

[18] J. Fukae, M. Takanashi, S. Kubo, K. Nishioka, Y. Nakabeppu, H. Mori, Y. Mizuno, N. Hattori, Expression of 8-oxoguanine DNA (OGG1) in Parkinson's disease and related neurodegenerative disorders, Acta Neuropathol., in press.

[19] P.H. Jensen, K. Islam, J. Kenny, M.S. Nielsen, J. Power, W.P. Gai, Microtubule-associated protein 1B is a component of cortical Lewy bodies and binds α-synuclein filaments, J. Biol. Chem. 275 (2000) 21500–21507.

[20] H.J. Rideout, K.E. Larsen, D. Sulzer, L. Stefanis, Proteasomal inhibition leads to formation of ubiquitin/α-synuclein-immunoreactive inclusions in PC12 cells, J. Neurochem. 78 (2001) 899–908.

[21] M.J. May, F. D'Acquisto, L.A. Madge, J. Glockner, J.S. Pober, S. Ghosh, Selective inhibition of NF-κB activation by a peptide that blocks the interaction of NEMO with the IκB kinase complex, Science 289 (2000) 1550–1554.

[22] D. Derossi, A.H. Joliot, G. Chassaing, A. Prochiantz, The third helix of the Antennapedia homeodomain translocates through biological membranes, J. Biol. Chem. 269 (1994) 10444–10450.

[23] H. Hall, E.J. Williams, S.E. Moore, F.S. Walsh, A. Prochiantz, P. Doherty, Inhibition of FGF-stimulated phosphatidylinositol hydrolysis and neurite outgrowth by a cell-membrane permeable phosphopeptide, Curr. Biol. 6 (1996) 580–587.

[24] M.J. May, R.B. Marienfeld, S. Ghosh, Characterization of the IκB-kinase NEMO binding domain, J. Biol. Chem. 277 (2002) 45992–46000.

[25] T. Ohuchida, K. Okamoto, K. Akahane, A. Higure, H. Todoroki, Y. Abe, M. Kikuchi, S. Ikematsu, T. Muramatsu, H. Itoh, Midkine protects hepatocellular carcinoma cells against TRAIL-mediated apoptosis through down-regulation of caspase-3 activity, Cancer 100 (2004) 2430–2436.

[26] Y. Imai, M. Soda, T. Murakami, M. Shoji, K. Abe, R. Takahashi, A product of the human gene adjacent to parkin is a component of Lewy bodies and suppresses Pael receptor-induced cell death, J. Biol. Chem. 278 (2003) 51901–51910.

[27] E. Lindersson, R. Beedholm, P. Hojrup, T. Moos, W. Gai, K.B. Hendil, P.H. Jensen, Proteasomal inhibition by α-synuclein filaments and oligomers, J. Biol. Chem. 279 (2004) 12924–12934.

[28] K.S. McNaught, P. Shashidharan, D.P. Perl, P. Jenner, C.W. Olanow, Aggresome-related biogenesis of Lewy bodies, Eur. J. Neurosci. 16 (2002) 2136–2148.
[29] K.S. McNaught, C. Mytilineou, R. Jnobaptiste, J. Yabut, P. Shashidharan, P. Jennert, W.C. Olanow, Impairment of the ubiquitin–proteasome system causes dopaminergic cell death and inclusion body formation in ventral mesencephalic cultures, J. Neurochem. 81 (2002) 301–306.
[30] H. Mori, J. Kondo, Y. Ihara, Ubiquitin is a component of paired helical filaments in Alzheimer's disease, Science 235 (1987) 1641–1644.
[31] C. O'Farrell, D.D. Murphy, L. Petrucelli, A.B. Singleton, J. Hussey, M. Farrer, J. Hardy, D.W. Dickson, M.R. Cookson, Transfected synphilin-1 forms cytoplasmic inclusions in HEK293 cells, Brain Res. Mol. Brain Res. 97 (2001) 94–102.
[32] F.P. Marx, C. Holzmann, K.M. Strauss, L. Lei, O. Eberhardt, E. Gerhardt, M.R. Cookson, D. Hernandez, M.J. Farrer, J. Kachergus, S. Engelender, C.A. Ross, K. Berger, L. Schols, J.B. Schulz, O. Riess, R. Kruger, Identification and functional characterization of a novel R621C mutation in the synphilin-1 gene in Parkinson's disease, Hum. Mol. Genet. 12 (2003) 1223–1231.

Available online at www.sciencedirect.com
SCIENCE DIRECT®
ELSEVIER
Biochemical and Biophysical Research Communications 332 (2005) 233–240
BBRC
www.elsevier.com/locate/ybbrc

Common anti-apoptotic roles of parkin and α-synuclein in human dopaminergic cells

Yutaka Machida [a,b], Tomoki Chiba [b], Atsushi Takayanagi [f], Yoshikazu Tanaka [b,c], Masato Asanuma [d], Norio Ogawa [d], Akihiko Koyama [e], Takeshi Iwatsubo [e], Shosuke Ito [h], Poul Hening Jansen [g], Nobuyoshi Shimizu [f], Keiji Tanaka [b], Yoshikuni Mizuno [a], Nobutaka Hattori [a,*]

[a] *Department of Neurology, Juntendo University School of Medicine, Tokyo, Japan*
[b] *Department of Molecular Oncology, The Tokyo Metropolitan Institute of Medical Science, Tokyo, Japan*
[c] *Department of Veterinary Hygiene, Nippon Veterinary and Animal Science University, Tokyo, Japan*
[d] *Department of Brain Science, Okayama University Graduate School of Medicine and Dentistry, Okayama, Japan*
[e] *Department of Neuropathology and Neuroscience, Graduate School of Pharmaceutical Sciences, University of Tokyo, Japan*
[f] *Department of Molecular Biology Keio University, Tokyo, Japan*
[g] *Department of Neurology, Zlekenhuls Gelderse Vallei, Edo, Netherlands*
[h] *Fujita Health University School of Health Sciences, Aichi, Japan*

Received 17 April 2005
Available online 30 April 2005

Abstract

Parkin, a product of the gene responsible for autosomal recessive juvenile parkinsonism (AR-JP), is an important player in the pathogenic process of Parkinson's disease (PD). Despite numerous studies including search for the substrate of parkin as an E3 ubiquitin–protein ligase, the mechanism by which loss-of-function of parkin induces selective dopaminergic neuronal death remains unclear. Related to this issue, here we show that antisense knockdown of parkin causes apoptotic cell death of human dopaminergic SH-SY5Y cells associated with caspase activation and accompanied by accumulation of oxidative dopamine (DA) metabolites due to auto-oxidation of DOPA and DA. Forced expression of α-synuclein (α-SN), another familial PD gene product, prevented accumulation of oxidative DOPA/DA metabolites and cell death caused by parkin loss. Our findings indicate that both parkin and α-SN share a common pathway in DA metabolism whose abnormality leads to accumulation of oxidative DA metabolites and subsequent cell death.

Keywords: Parkin; Apoptosis; Antisense; Knockdown; Neuroblastoma; Synuclein dopamine metabolism; Quinone

Parkinson's disease (PD) is the second most common neurodegenerative disorder primarily caused by selective loss of dopaminergic neurons in the midbrain substantia nigra pars compacta. Familial PD has been highlighted to study the mechanisms underlying neurodegeneration in PD, although only 5–10% of patients with PD are of the familial form of PD [1,2]. To date, 10 causative genes have been mapped and cloned in familial PD by linkage studies, which have significantly enhanced our understanding of the genetic mechanisms of PD [3]. Of these genes, *parkin*, the causative gene (*PARK2*) of AR-JP, representing the most prevalent form of familial PD [4], is of special interest, because it encodes an E3 ubiquitin–protein ligase [5], which

* Corresponding author. Fax: +81 3 5800 0547.
E-mail address: nhattori@med.juntendo.ac.jp (N. Hattori).

0006-291X/$ - see front matter © 2005 Elsevier Inc. All rights reserved.
doi:10.1016/j.bbrc.2005.04.124

covalently attaches ubiquitin to target proteins, designating them for destruction by the proteasome [6,7]. These findings suggest that impediment of *parkin* leads to deterioration of dopaminergic neurons and that PD, at least AR-JP, is caused by the failure of proteolysis mediated by the ubiquitin–proteasome system [8]. Since then, our knowledge about parkin has expanded, and indeed at present various putative substrates, e.g., CDCrel-1, synphilin-1, α-SN22 (O-glycosylated form of α-synuclein [α-SN]), Pael-R, and cyclin E have been identified [9–14]. Moreover, negative regulation of parkin E3 activity by parkin modification, such as nitration and phosphorylation, has been reported [15–17], but the pathophysiological role of parkin is still poorly understood.

One crucial issue that needs to be investigated is why AR-JP brains show severe neuronal loss with gliosis in the substantia nigra and mild neuronal loss in the locus coeruleus and why dopaminergic neurons in the substantia nigra are particularly vulnerable to the loss-of-function effect of parkin, though parkin is expressed ubiquitously throughout the brain. To define how the loss-of-function of parkin induces selective dopaminergic neuronal death in the midbrain, we interfered with endogenous parkin mRNA, a potentially suitable in vitro model of AR-JP for investigating the mechanism of selective dopaminergic neuronal death. To knock down the level of parkin in cells, we designed a full-length human parkin antisense (abbreviated as-parkin) using an adenovirus vector that has a high multiplicity of infection (moi) toward post-mitotic cells or cell lines which has neuronal characteristics and is an excellent tool to search for the effect of as-parkin on differentiated SH-SY5Y cells that exhibit features characteristic of dopaminergic neurons.

Here, we report that as-parkin selectively induced apoptosis of SH-SY5Y cells in a caspase-dependent manner. We also found that loss of parkin resulted in accumulation of endogenous L-3,4-dihydroxyphenylalanine (DOPA)- and dopamine (DA)-chromes derived from auto-oxidation of DOPA/DA-quinones, which mediates the toxic effect by covalently binding to the thiol group of proteins and consequently disintegrates cellular integrity and eventually causes cell death [18–20]. α-SN is a putative protein associated with membrane transport or signal transduction but of unknown function. α-SN gene mutations such as missense or multiplication cause familial autosomal dominant PD [21–27]. We found that forced expression of α-SN suppressed the loss of cell viability and accumulation of oxidative DOPA/DA metabolites caused by loss of parkin. Based on these findings, we propose that parkin and α-SN contribute to a common DA metabolic pathway; the impairment of which may lead to selective degeneration of dopaminergic neurons and consequently to PD.

Materials and methods

Adenoviruses. We used the adenoviral plasmid (pAdEasy-1) and the shuttle vector (p-shuttle-CMV) (Q.Bio gene). Various cDNAs used were inserted into the shuttle vector. The shuttle vector plasmid was linearized with *Pme*I. Electrocompetent *Escherichia coli* BJ5183 cells were added and electroporation was performed in 2-mm cuvettes in a Gene Pulser electroporator. Cells were inoculated onto 10-cm Petri dish containing LB-agar and 50 μg/ml kanamycin. Smaller colonies were picked and grown in 2 ml LB-broth (Sigma Chemical St. Louis, MO) containing 50 μg/ml kanamycin. Recombination was confirmed with *Pac*I. Approximately 5×10^6 cells were plated onto 10-cm culture dish. Ten micrograms of plasmid DNA linearized by *Pme*I, 12 μl FuGENE6 (Roche Molecular Systems, NJ), and 500 μl OptiMEM (Gibco-BRL) were mixed and transfected, according to the protocol provided by the manufacturer. After 7–10 days, the cells were collected by scraping off the 10-cm dish together with floating cells in the culture. The supernatant was removed after low-speed centrifugation. After sonicating the pellet, the cells were resuspended into 1 ml Dulbecco's modified Eagle's medium (DMEM) and frozen to −80 °C. In the next step, 500 μl of viral lysate was used to infect 7×10^7 cells in 15-cm dish. This process was repeated 1–3 times. Viruses were purified by CsCl banding; the final yield was 10^{10} plaque forming units.

Cells and cell culture. Human neuroblastoma cells (SH-SY5Y) and HeLa cells were obtained from American Type Culture Collection. The cells were maintained in growth medium (DMEM, Sigma, supplemented with 10% fetal bovine serum [Gibco-BRL, Gaithersburg, MD], 100 U/ml penicillin, and 100 μg/ml streptomycin) at 37 °C under 5% CO_2. SH-SY5Y cells were cultured with 100 μM of all *trans*-retinoic acid in dimethyl sulfoxide (DMSO) (Sigma R-2625) for 3 to 4 days for differentiation. The cells were infected with the antisense adenovirus at 150 moi; LacZ at 150 and 5 moi, wild and mutant α-SN adenovirus at 5 moi. Cells were collected 36 h after infection, centrifuged, and analyzed.

Western blotting. Infected or control cells were lysed in Laemmli SDS sample buffer. Proteins were separated by sodium dodecyl sulfate–polyacrylamide gel electrophoresis (SDS–PAGE) (NuPAGE, Invitrogen, San Diego, CA) and transferred onto polyvinylidene difluoride (PVDF) membrane. Western blotting was performed according to the ECL protocol provided by the supplier (Invitrogen, San Diego, CA) using specific antibodies of parkin and cleaved caspases (Cell Signaling Technology, Beverly, MA), α-SN (BD Transduction Laboratories, Lexington, KY), and β-Gal (Promega, Madison, WI).

Cell survival assay. Cells were infected with as-parkin or LacZ adenovirus and incubated for 48 h in 96-well plate. Cell viability was evaluated using the WST8, MTT reduction assay. Briefly, the solution of 0.1 mg/ml MTT in DMEM was added to each well and incubated for 2 h. The transmission was evaluated at 450 and 655 nm by 96-well microplate reader (Bio-Rad, Richmond, CA).

TUNEL assay. Terminal-deoxynucleotidyl transferase mediated d-UTP nick end labeling (TUNEL) assay was performed using formalin-fixed, ApopTag In Situ Apoptosis Detection Kits (Intergen, Purchase, NY). Fragmented DNA was labeled by fluorescein isothiocyanate (FITC) and observed under a fluorescence microscope.

Measurements of DOPA/DA-chromes. Thirty-six hours after infection, cells were solubilized in 500 μl of 1% Triton X-100 solution for 2 h and then centrifuged at 20,000*g* for 30 min at 4 °C. The supernatant was used as cell extract and was incubated for 3 min at room temperature. After 10% TCA protein precipitation, the generation of DOPA/DA-quinones was estimated by measuring the absorbance of the incubation supernatant at 475 nm based on the formation of DOPA/DA-chromes. The amount of DOPA/DA-chromes was calculated from a standard curve constructed using known amounts of DA and 0.01 mg/ml tyrosinase. The protein concentration in the cell extracts was determined by using the BCA Protein Assay Reagent Kit

(Pierce Chemical, Rockford, IL) with bovine serum albumin as a standard.

Statistical analysis. All data were expressed as means ± SEM. Differences between groups were examined for statistical significance using Dunnett's t test or Turkey's multiple t test. A P value less than 0.05 denoted the presence of a statistically significant difference.

Results and discussion

Antisense parkin causes loss of viability of SH-SY5Y cells

We first examined the effect of knockdown of parkin on the viability of human neuroblastoma cells (SH-SY5Y). These cells contain dopaminergic machinery and can differentiate into neuronal-like phenotypes when treated for 3–5 days with retinoic acid (RA), accompanied by arrest of cell proliferation and increased dopamine metabolism [28,29]. Infection of SH-SY5Y with full-length human as-parkin adenovirus caused deterioration of cell viability, as monitored by 3-(4,5-dimethylthiazol-2-yl)-2,5-diphenyltetrazolium bromide (MTT) reduction assay. The differential SH-SY5Y cell death effect was observed in the range between 50 and 250 moi titer of as-parkin adenovirus (data not shown) and thereafter we routinely used 150 moi titer (Fig. 1A, left panel). Control β-galactosidase (β-Gal) adenovirus had no effect on cell viability, although β-Gal was highly expressed in SH-SY5Y cells (Fig. 1A, right panel). Infection of cells with as-parkin caused a marked decrease of endogenous parkin protein level in differentiated SH-SY5Y cells, without altering actin level in the cells (Fig. 1A, right panel). The effect of as-parkin was abrogated, upon co-infection with sense-parkin (data not shown).

Effect of antisense parkin is cell-type specific

Intriguingly, we found that the effect of as-parkin on cell viability was much less in undifferentiated growing SH-SY5Y cells compared with differentiated cells (Fig. 1B, left panel). In addition, as-parkin did not influence cell viability of HeLa cells derived from human adenocarcinoma of the uterine cervix, which do not express parkin protein and lack the dopamine metabolic pathway (Fig. 1B, right panel). Thus, antisense knockdown of parkin exerts its effect based on the cell type, and the effects are observed in a dopaminergic neuron-specific manner, and depend on the differentiation state of dopaminergic neurons.

Antisense parkin induces apoptotic cell death

As shown in Fig. 1C, the cells appeared clear when their morphology was compared with uninfected (control) and β-Gal expressing cells. SH-SY5Y cells infected with as-parkin adenovirus showed morphological

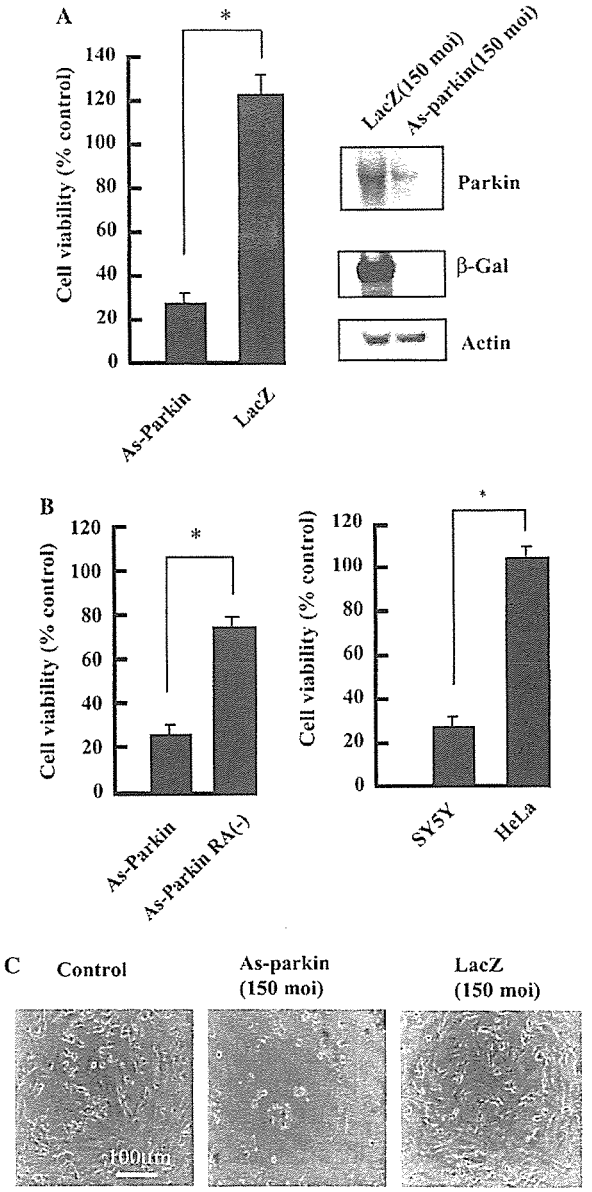

Fig. 1. Parkin knockdown is associated with loss of SH-SY5Y cell viability. (A) Effects of antisense parkin (as-parkin) and LacZ. Adenoviruses were infected for 48 h with 150 moi titers as indicated on the differentiated SH-SY5Y cells that had been pre-cultured with RA for 4 days. Cell viability was determined by the MTT assay (left panel). The results are expressed as percentage of MTT activity of uninfected cells (control). Data represent means ± SEM of 8 determinations. $*P < 0.01$ versus control group (Dunnett's t test). Cells that had been treated for 48 h with 150 moi titers of as-parkin and LacZ adenoviruses were lysed in Laemmli SDS sample buffer, and the proteins were separated by SDS–PAGE, followed by Western blotting with antibodies against parkin, β-galactosidase (β-Gal), and actin (right panel). (B) Undifferentiated SH-SY5Y cells without treatment with RA and HeLa cells were treated for 48 h with as-parkin adenovirus. The cell viability was measured and represented as indicated. (C) Morphological changes in differentiated SH-SY5Y cells upon knockdown of parkin. The cells were infected for 48 h with as-parkin and LacZ adenovirus vectors or left uninfected (control). Note the presence of apoptotic cells. Bar, 100 μm.

changes typical of apoptosis. To determine the nature of cell death induced by as-parkin, we performed TUNEL assay. As shown in Fig. 2A, as-parkin-treated SH-SY5Y cells showed nuclear condensation and fragmentation. In contrast, these changes were rarely observed in β-Gal-expressing SH-SY5Y cells. In support

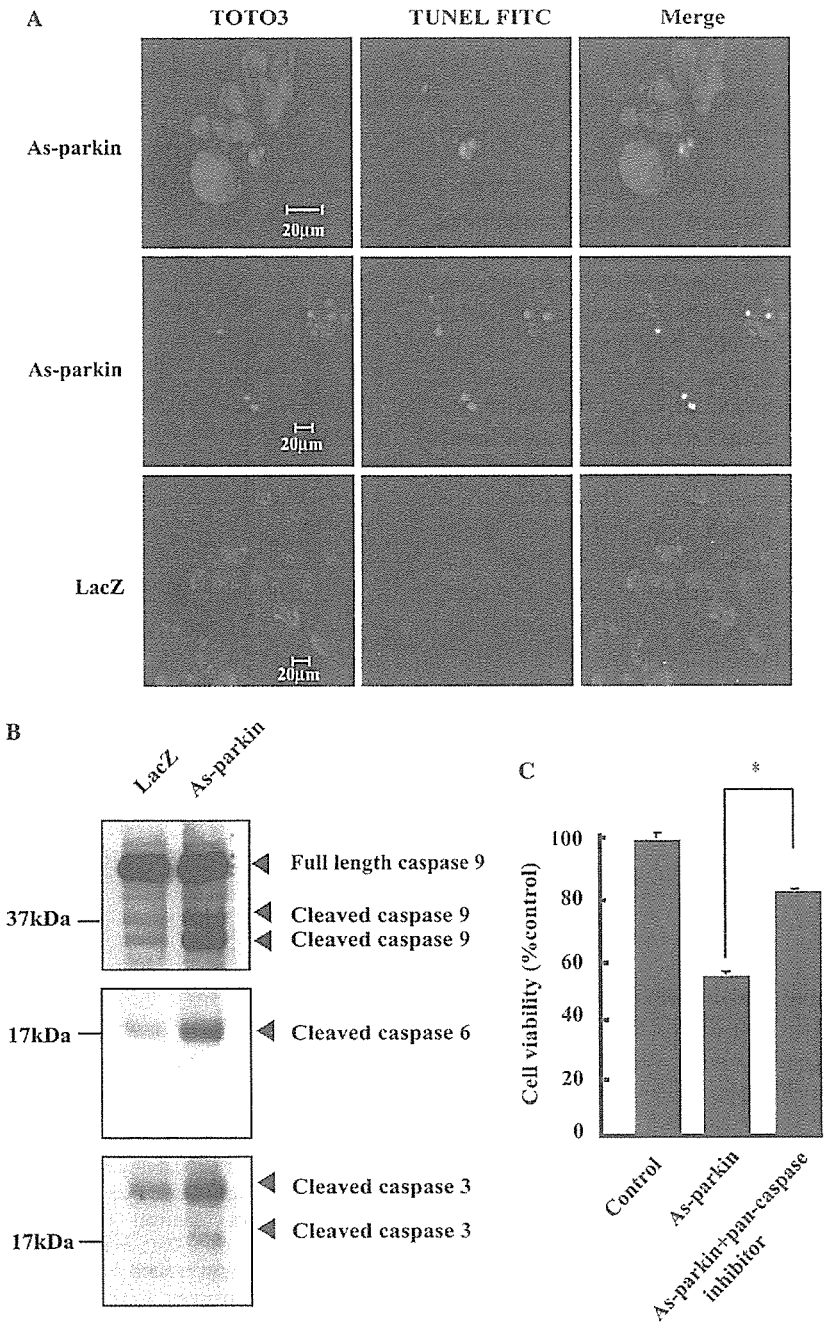

Fig. 2. Parkin knockdown induces apoptosis. (A) Detection of cells with nuclear DNA fragmentation due to parkin knockdown by TUNEL assay. Differentiated SH-SY5Y cells were treated for 48 h with as-parkin and LacZ adenoviruses (150 moi). TUNEL assay was performed to detect apoptotic cells. TUNEL-positive cells (green) were detected (TdT enzyme is labeled with FITC green fluorescence). Nuclei were counterstained with TOTO3 (red). Bar, 20 μm. (B) Activation of caspase-3, -6, and -9 by as-parkin. After infection with as-parkin and LacZ adenoviruses as for a, the cell extracts were used for Western blot analysis using antibodies against cleaved caspase-3, -6, and -9. Arrowheads on the right indicated corresponding caspases. Note that anti-cleaved caspase-3 and -6 antibodies did not react with their native forms. (C) Effects of a 'pan' caspase inhibitor on apoptosis induced by the loss of parkin. The inhibitor was added at 100 μM when cells were treated by as-parkin adenovirus as for (A). Note that the caspase inhibitor significantly blocked parkin knockdown-induced deterioration of cell viability. Data represent means ± SEM of 8 determinations. $^{*}P < 0.05$ versus control (uninfected) group (Dunnett's t test).

of the TUNEL findings, we also detected activation of caspase-3, -6, and -9 in SH-SY5Y cells under parkin knockdown (Fig. 2B). In addition, Western blot analysis showed cleaved poly(ADP)-ribose polymerase (PARP) in the course of as-parkin infection and a time-dependent increase of the 25-kDa cleaved fragment, confirming the activation of caspase(s) (data not shown). Further experiments showed that application of a pan-caspase inhibitor for 6 h before infection significantly prevented apoptotic cell death as determined by the MTT reduction assay (Fig. 2C). Taken together, these results suggest that as-parkin-induced SH-SY5Y cell death is likely to be mediated by activation of the caspase cascade.

Antisense parkin increases DOPA/DA metabolites

Next we examined the effect of α-SN on the viability and DOPA/DA-chrome level in differentiated SH-SY5Y cells with a reference to parkin loss. These experiments were based on previous studies describing abnormal DA metabolism in α-SN-deficient mice [30] and α-SN binding to DA-quinones [31]. For this purpose, we constructed adenovirus vectors expressing α-SN, and first tested its effect on the expression of parkin. α-SN and its PD-linked mutants (Ala30Pro and Ala53Thr) had no effect on the levels of parkin, irrespective of the treatment of as-parkin (Figs. 4A and B). It is of note that α-SN did not express at significant levels in SH-SY5Y cells under present conditions. Then, we investigated the effect of α-SN on the as-parkin-induced loss of cell viability. As shown in Fig. 4A, infection of SH-SY5Y cells by both adenovirus vectors expressing α-SN and as-parkin caused marked reduction of their cellular chrome levels and resulted in amelioration of as-parkin-induced deterioration of cell viability (Fig. 4B). Intriguingly, coinfection of cells with wild-type α-SN and as-parkin adenoviruses abrogated as-parkin-induced accumulation of DOPA/DA-chrome. However, α-SN mutants (Ala30Pro and Ala53Thr) and β-Gal expression did not reduce the generation of DOPA/DA-chrome by as-parkin. Thus, it seems that the α-SN-induced suppression of apoptosis was associated with a reduction in the DOPA/DA-chrome level in α-SN expressing SH-SY5Y cells. These results suggest that α-SN inhibits apoptosis induced by parkin knockdown by blocking the generation of DOPA/DA-chromes; i.e., DOPA/DA-quinones.

Antisense parkin-induced extensive apoptosis of differentiated dopaminergic SH-SY5Y cells but limited apoptosis of undifferentiated SH-SY5Y cells and no apoptosis of HeLa cells, indicating cell-type specificity. With regard to the cell-specific vulnerability, an important factor seems to be dopamine (DA) metabolism, which is a peculiar feature of dopaminergic neurons. Indeed, the differentiated SH-SY5Y cells retain a high DA metabolic pathway [28,29]. DA is a molecule prone to oxidation and it contributes to the generation of reactive oxygen species, which when in abundance can cause oxidative injury of various cellular components[18,20]. Indeed, abnormally high levels of these free radicals in dopaminergic neurons have been implicated as environmental factors causing not only sporadic PD but also AR-JP [32,33]. We tested the effects of as-parkin infection on the level of endogenous DOPA- and DA-chromes (DOPA/DA-chromes), which are derived from DOPA- and DA-quinones, respectively, whose metabolites could originate from cytosolic DOPA or DA oxidation [18,20]. Thus, the amounts of DOPA/DA-chromes reflect those of endogenous DOPA/DA-quinones. DOPA/DA-chrome levels were significantly high in parkin knockdown cells whereas there was no change in β-Gal expressing ones (Fig. 4A). These findings suggest that parkin knockdown-induced apoptosis is mediated by an increase in DOPA/DA-chromes.

Recently, four groups independently reported the generation of a mouse model that lacks the *parkin* gene, which display certain abnormalities of dopamine metabolism [34–37]. However, these parkin knockout mice had only subtle phenotypes exhibiting a largely normal gross brain morphology. Based on the pathologic findings, all the parkin null mice showed no neuronal loss in the SN. This is in marked contrast to our in vitro system described in this study, in which parkin knockdown induced activation of the caspase cascade and apoptosis of dopaminergic SH-SY5Y cells. Why do parkin knockout mice lack the abnormalities seen in AR-JP patients? One plausible explanation is the presence of a putative molecule(s) that suppresses the defect induced by loss-of-function of parkin, and the abundant presence of such molecule(s) in the brain should be linked to the pathogenesis of PD. Here, we propose that α-SN is the molecule that compensates for the loss of parkin, since α-SN prevented apoptotic cell death induced by as-parkin. In this regard, Western blot analysis showed that the dopaminergic SH-SY5Y cells did not express α-SN at significant levels (Fig. 3A, lanes 2 and 4), which is in marked contrast to the high abundance of dopaminergic neurons in vivo [38]. Regardless of the compensatory role of α-SN for the loss-of-function of parkin in the AR-JP, α-SN probably cannot cope with the accumulation of toxic molecules in the absence of parkin and thus apoptotic neuronal death perhaps occurs gradually, leading to degeneration of dopaminergic neurons and consequently the development of early-onset PD. We provide the first evidence for the anti-apoptotic role of α-SN and its involvement in the common pathway of parkin.

To date, several studies have demonstrated that α-SN exerts protective effects against various cellular stresses such as oxidative damage and related apoptosis of neurons [39,40]. Considering the reason why muta-